creative commons
COMMONS DEED

저작자표시-비영리-변경금지 2.0 대한민국

이용자는 아래의 조건을 따르는 경우에 한하여 자유롭게

- 이 저작물을 복제, 배포, 전송, 전시, 공연 및 방송할 수 있습니다.

다음과 같은 조건을 따라야 합니다:

저작자표시. 귀하는 원저작자를 표시하여야 합니다.

비영리. 귀하는 이 저작물을 영리 목적으로 이용할 수 없습니다.

변경금지. 귀하는 이 저작물을 개작, 변형 또는 가공할 수 없습니다.

- 귀하는, 이 저작물의 재이용이나 배포의 경우, 이 저작물에 적용된 이용허락조건을 명확하게 나타내어야 합니다.
- 저작권자로부터 별도의 허가를 받으면 이러한 조건들은 적용되지 않습니다.

저작권법에 따른 이용자의 권리는 위의 내용에 의하여 영향을 받지 않습니다.

이것은 이용허락규약(Legal Code)을 이해하기 쉽게 요약한 것입니다.

Disclaimer

dCollection

이학박사 학위논문

Simple and Efficient Fabrication of Dimers of Metal Colloidal Particles for Surface-Enhanced Raman Scattering and their Applications

금속 이중합체 제조를 통한 표면 증강 라만 산란 연구와 응용

2018년 2월

서울대학교 대학원

화학부 물리화학

윤 혁 진

Simple and Efficient Fabrication of Dimers of Metal Colloidal Particles for Surface-Enhanced Raman Scattering and their Applications

지도 교수 서 정 쌍

이 논문을 이학박사 학위논문으로 제출함
2017년 6월

서울대학교 대학원
화학부 물리화학전공
윤 혁 진

윤혁진의 이학박사 학위논문을 인준함
2017년 6월

위 원 장 김 지 환 (인)

부위원장 서 정 쌍 (인)

위 원 이 성 훈 (인)

위 원 정 대 홍 (인)

위 원 주 상 우 (인)

Abstract

Hyeokjin Yoon
Department of Chemistry, Physical Chemistry
The Graduate School
Seoul National University

Since the advent of surface-enhanced Raman scattering (SERS), researchers have been trying to fabricate highly sensitive, easy to make and stable SERS substrates. This thesis introduces a simple and efficient method to fabricate SERS substrates consisting mainly of dimers of Ag or Au colloidal particles by controlling the surface charge of the particles. The surface charge was controlled from the pristine colloidal solutions by centrifuging. The SERS substrates were fabricated by a three-step immobilization method as follows: immobilization of the colloidal particles, adsorption of target molecules on the immobilized colloidal particles, and second immobilization. The morphology of the SERS substrates was examined by scanning electron spectroscopy and characterized by UV-vis spectroscopy. For the optimized SERS substrates based on Ag sols, the average enhancement factor was calculated to be ~6.1×10^7.

The size effect of colloidal silver particles to SERS enhancements was studied. The silver nanoparticles (NPs) were synthesized through a seed-mediated method. Silver seeds whose size was ranged from approximately 5 to 10 nm were prepared by adding a sodium borohydride solution into a silver nitrate solution containing sodium citrate. The isotropic growth of Ag seed NPs was initiated by adding growth solutions containing appropriate amounts of silver nitrate and sodium ascorbate as a reducing agent into the seed solution. By adjusting the volume ratio of the seed solution to the growth solution, the size of silver NPs was controlled. Using this method, four silver colloidal solutions containing silver NPs whose average diameters were 21, 25, 28, and 31 nm were prepared. The size and shape of silver NPs were examined by transmission electron microscopy. The surface plasmon absorption band due to the longitudinal mode was red-shifted with increasing the average diameter of Ag NPs. The SERS intensity measured by excitation with 514.5 nm laser light was critically affected by the diameter of Ag NPs. The highest SERS intensity was measured from the substrate whose absorption

maximum due to the longitudinal mode was near 519 nm. The SERS substrate made of 28 nm Ag NPs showed higher enhancement than that made of 21, 25 or 31 nm Ag NPs.

The percentage of intensity contributed by the molecules located at the junctions to the total SERS intensity was calculated to be ~85% from the enhancement difference between two kinds of substrates prepared by three- and four-step methods. The four-step method is as follow: immobilization of the colloidal particles, adsorption of aniline on the immobilized nanoparticles, second immobilization, and adsorption of target molecules on the nanoparticles. The enhancement at the junctions, which acted as the hotspots, was found to be $\sim 3 \times 10^{9}$.

Furthermore, the substrate prepared by adsorbing aniline (four-step method) worked as a universal SERS substrate. When target molecular solutions (adenosine, guanine, glycine, rhodamine 6G, benzoic acid, 4-aminothiophenol) were dropped in arrays on the substrate and then dried, a good SERS spectrum was observed from each spot, with an enhancement factor of $\sim 9.1 \times 10^{6}$.

Keywords

Surface-enhanced Raman Scattering(SERS), Noble Metal Nanoparticle, Localized Surface Plasmon Resonance(LSPR), Dimer, Plasmonics, Raman spectroscopy.

Student number 2013-30906

Table of Contents

Abstract i

Table of Contents v

List of Figures viii

List of Tables xvi

Chapter 1. Introduction 1

1.1. Surface-Enhanced Raman Scattering 1

1.1.1. Raman Spectroscopy 1

1.1.2. Surface-Enhance Raman Scattering 3

1.1.3. Applications of SERS 4

1.1.3.1. In Vivo Applications of SERS 4

1.1.3.2. In Vitro Applications of SERS 8

1.1.3.3. Graphene-Enhanced Raman Scattering (GERS) 9

1.2. Plasmonic Nanoparticles 11

1.2.1. Surface Plasmon Resonance 11

1.2.2. Noble Metal Nanoparticles 12

1.2.3. SilverNanoparticles 13

1.2.4. Gold Nanoparticles 13

Chapter 2. Experimental Section 14

2.1. Materials 14

2.2. Size-Controlled Synthesis of Silver Nanoparticles 14

2.2.1. Preparation of Silver Seeds 14
2.2.2. Seeded Growth of Silver Nanoparticles 15
2.3. Synthesis of Gold Nanoparticles.....16
2.3.1. Preparation of Gold Seeds.....16
2.3.2. Seeded Growth of Gold Nanoparticles 16
2.4. Fabrication of Nanoclusters on a Cover Glass for SERS...17
2.5. Characterization.....20
2.5.1. TEM 20
2.5.2. SEM.....20
2.5.3. UV-visible Spectroscopy 20
2.5.4. Raman Spectroscopy 20

Chapter 3. Dimer of Noble Metal Nanoparticles.....22
3.1. Materials 22
3.1.1. Synthesis and Characterization of the Noble Metal NPs22
3.1.2. Fabrication of Dimers of Metal Colloidal Particles.....26
3.2. Conclusions.....41

Chapter 4. Effect of Particle Diameter on Surface-Enhanced Raman Scattering.....43

Chapter 5. Calculating the Enhancements inside and outside of Ag Dimers 47

5.1. Results and Discussion.....48
5.2. Conclusions.....70

Chapter 6. Universal SERS-substrates.....71
6.1. Results and Discussion.....72
6.2. Conclusions.....85

References.....86
Abstract in Korean.....94

List of Figures

Figure 1. Schematic identifying light scattering after laser exposure on a sample surface.[1].....2

Figure 2. TEM images of B60 nm gold nanostars (A), a single gold nanostar (B) and one of its tips (C) at larger magnification. [5].....5

Figure 3. (A) White light image of a prostate tissue specimen with an overlaid SERS false color image based on the intensity of the 1340 cm−1 Raman marker band of the SERS label. (B) Five representative SERS spectra from different locations in (A), indicated by white crosses in the SERS false color image (from top to bottom).[5].....6

Figure 4. In vivo cancer targeting and surface− enhanced Raman detection by using ScFv− antibody conjugated gold nanoparticles that recognize the tumor biomarker EGFR. (a,b)SERS spectra obtained from the tumor and the liver locations by using targeted (a) and nontargeted (b) nanoparticles. Two nude mice bearing human head−and−neck squamous cell carcinoma (Tu686) xenograft tumor (3−mm diameter) received 90 ml of ScFv EGFR−conjugated SERS tags or pegylated SERS tags (460 pM). The particles were administered via tail vein single injection. SERS spectra were taken 5 h after injection. (c) Photographs showing a laser beam focusing on the tumor site or on the anatomical location of liver. In vivo SERS spectra were obtained from the tumor site (red) and the liver site (blue) with 2−s signal integration and at 785 nm excitation. The spectra were background subtracted and

shifted for better visualization. The Raman reporter molecule is malachite green, with distinct spectral signatures as labeled in a and b. [6]....8

Figure 5. Schematic of SERS array for matrix metalloproteinase-7 (MMP-7) and carbohydrate antigen 19-9 (CA 19-9).[10]....9

Figure 6. (a) Schematic illustration of the molecules on graphene and a SiO2/Si substrate, and the Raman experiments. (b-d) are the comparisons of Raman signals of Pc deposited 2 Å on graphene (red line) and on the SiO2/Si substrate (blue line) using vacuum evaporation at 632.8 nm excitation (b), 514.5 nm excitation (c), and 457.9 nm excitation (d).[11]....10

Figure 7. Schematic illustration of (A) localized and (B) propagating surface plasmon polaritons. E depicts the electric field vector and k the wave vector.[25]....12

Figure 8. Schematic illustration of preparation of silver nanoparticles. 15

Figure 9. Schematic illustration of the preparation of gold nanoparticles....17

Figure 10. Schematic of the fabrication of SERS substrates consisting of dimers of metal colloidal particles; (a) immobilization of the colloidal particles on a cover glass coated with P4VP, (b) adsorption of target molecules (adsorbates), and (c) second immobilization....19

Figure 11. (a-e) SEM images and (f) extinction spectra of Ag (a-d) NPs and (f) seeds. 24

Figure 12. Normalized extinction spectra of Au NPs. The legend shows growth step.....25

Figure 13. TEM image of Au NPs after 2nd growth step. The average diameter of Au NPs is about 50 nm.....26

Figure 14. (a–d) SEM images of the substrates fabricated from purified silver sols by the three–step immobilization process with various second immobilization times and (e) histogram of the number of Ag colloidal clusters counted from the SEM images. The first immobilization time was all the same as 10 min and the second immobilization times were (a) 0, (b) 10, (c) 20, and (d) 30 min. The total amount of benzenethiol adsorbed was all the same for all substrates. The average diameter of the immobilized Ag colloidal particles was about 28 nm.....30

Figure 15. (a) UV–Vis extinction spectra and (b) benzenethiol SERS spectra measured from the substrates fabricated under the same conditions as used in the fabrication of the substrates for Figure 1. The legend shows the second immobilization times. A 514.5 nm Ar–ion laser line was used as the excitation source. The acquisition time was 1 s.....33

Figure 16. SERS spectra of benzenethiol obtained at 10 randomly selected positions within the substrate prepared by the three–step method. The acquisition time was 1 s.....34

Figure 17. SEM images, UV–Vis extinction spectra, and benzenethiol SERS spectra of the substrates prepared using pristine, not purified, Ag sols by the three–step immobilization process with

various second immobilization times, and histogram of the number of Ag colloidal clusters counted from the SEM images. The first immobilization time was 10 min and the second immobilization times were (a) 0, (b) 20, (c) 30, and (d) 60 min. The average diameter of the immobilized Ag colloidal particles was about 28 nm. The legend shows the second immobilization times. A 514.5 nm Ar-ion laser line was used as the excitation source. The acquisition time was 1 s.....37

Figure 18. (a) SERS spectra of benzenethiol adsorbed on the substrates at varying concentrations from 50 to 500 nM. (b) Enhancement factors of the substrates as a function of the concentration of benzenethiol solution. The acquisition time was 1 s.....39

Figure 19. SEM image of Au clusters immobilized on a cover glass coated with P4VP.....40

Figure 20. Extinction spectrum of Au dimers immobilized on a cover glass coated with P4VP.....41

Figure 21. Normalized UV-Vis extinction spectra measured from the substrates prepared by a three-step immobilization technique using purified Ag sols whose average diameter of colloidal particles were 22, 25, 28 and 31 nm. The legend represents the average diameters of Ag colloidal particles.....44

Figure 22. (a) UV-vis extinction spectra of the substrates Ag colloidal particles whose average diameters were 22, 25, 28, and 31 nm, and (b) SERS spectra of benzenethiol adsorbed on the

substrates prepared by the three-step immobilization technique using four different Ag nanoparticles in average diameter. The acquisition time was 1 s.....46

Figure 23. SEM image of the substrate after the first immobilization (a), and SEM images of two different SERS substrates prepared by the three-step (b) and four-step (c) immobilization methods. In both methods, the first and second immobilization times were the same as 10 and 30 min, respectively. The total amount of benzenethiol adsorbed on each substrate was the same. In the SEM image (a); there are 117 monomers. In the image (b); 75 monomers, 72 dimers, and 2 trimers. In the SEM image (c); 74 monomers, 77 dimers, and 2 trimers.....51

Figure 24. (a-b) SEM images, (c) UV-Vis extinction spectra, and (d) benzenethiol SERS spectra of the substrates prepared using pristine, not purified, Ag sols by the three-step immobilization process with various second immobilization times, and (d) histogram of the number of Ag colloidal clusters counted from the SEM images. The first and second immobilization times were 10 and 30 min, respectively. The average diameter of the immobilized Ag colloidal particles was about 28 nm. The legend shows the second immobilization times. A 514.5 nm Ar-ion laser line was used as the excitation source.....53

Figure 25. Comparison of (a) UV-Vis extinction and (b) SERS spectra measured from the two different substrates whose SEM images are shown in Figure 23. The black spectra were obtained

from the substrate prepared by the three-step method, while the red spectra from the substrate prepared by the four-step method. The total amount of benzenethiol adsorbed on each substrate was the same. The intensity of the black SERS spectrum was approximately 6.5 times stronger than that of the red SERS spectrum. The acquisition time was 1 s and the 50× objective lens was used. For two substrates, the total number of benzenethiol molecules adsorbed was the same and the adsorption time of benzenethiol was also the same as 24 h.....55

Figure 26. SERS spectra of benzenethiol obtained at 10 randomly selected positions within the substrate prepared by the four-step method. The acquisition time was 1 s.....56

Figure 27. SERS spectra of benzenethiol continuously measured 20 times at intervals of 10 seconds at a position within the substrate prepared by the four-step method. The acquisition time was 1 s..58

Figure 28. Comparison of the normal Raman spectrum of pure benzenethiol liquid with the SERS spectrum measured from the SERS substrate prepared by the three-step immobilization method. The acquisition time was 1 s. Spectra were acquired at 514.5 nm using a 10× objective (NA = 0.25).....63

Figure 29. Comparison of the normal Raman spectrum of pure benzenethiol liquid with the SERS spectrum measured from the SERS substrate prepared by the four-step immobilization method. The acquisition time was 1 s. Spectra were acquired at 514.5 nm using a 10× objective (NA = 0.25).....65

Figure 30. A schematic showing our approach to estimate the number of target molecules adsorbed on the surface of the junction of a dimer. The junction area is assumed to comprise a cap on the surface of each colloidal particle in the interparticle region of the dimer (red color).....69

Figure 31. (a–d) SEM images and (e) UV–Vis extinction spectra of substrates prepared by a three–step immobilization method and adsorption of aniline in the second step, and (f) histogram of the number of Ag colloidal clusters counted from the SEM images. The first immobilization time was all the same as 10 min, while the second immobilization times were (a) 0, (b) 20, (c) 30, and (d) 40 min. Purified silver sols whose colloidal particles had 28 nm in average diameter were used in the immobilizations. The legend shows the second immobilization times.....75

Figure 32. SERS spectra of benzenethiol measured from substrates prepared by a three–step immobilization method and adsorption aniline in the second step, after dipping each substrate in a 3.0 mL ethanol solution of 100 nM benzenethiol for 24 h and drying. The first immobilization time was all the same as 10 min, and the second immobilization time was varied. The legend shows the second immobilization times. A 514.5 nm Ar–ion laser line was used as the excitation source. The acquisition time was 1 s.....77

Figure 33. SERS spectra of benzenethiol obtained at 10 randomly selected positions within the substrates whose second immobilization time was (a) 10, (b) 20, (c) 30, and (d) 40 min. The

acquisition time was 1 s.....79

Figure 34. SERS spectra of several molecules measured from the spots after dropping target molecular solutions in arrays on the substrate, which was prepared by a three-step immobilization method and adsorbing aniline in the second step, and drying. The first and second immobilization times were 10 and 30 min, respectively. A 20 μL of target molecular solutions (100 nM) was dropped by using a micropipette. A 514.5 nm Ar-ion laser line was used as the excitation source. The acquisition time was 1 and 10 s for the bottom three molecules and the others, respectively..81

Figure 35. SERS spectra of several molecules, which were recorded from the substrates prepared by adsorbing aniline after dipping each substrate in a 3 mL of target molecule ethanol solution of each kind of target molecules. The first and second immobilization time were 10 and 30 min, respectively. Purified silver sols whose colloidal particles had 28 nm in average diameter were used in the immobilization steps. The concentration of target molecular solutions was all the same as 100 nM. A 514.5 nm Ar-ion laser line was used as the excitation source. The spectrum of aniline was observed from the substrate prepared by adsorption of aniline, without any dipping or dropping. The acquisition time was 10 s for adenosine, guanine, and glycine and 1 s for the others.....83

List of Tables

Table 1. Experimental evaluation of relative standard deviation (RSD) of SERS intensity on the substrates prepared by the three-step method.....34

Table 2. Experimental evaluation of relative standard deviation (RSD) of SERS intensity on the substrates prepared by the four-step method.....57

Table 3. Experimental evaluation of relative standard deviation (RSD) of SERS intensity on the four different substrates whose second immobilization time was (a) 10, (b) 20, (c) 30, and (d) 40 min.....80

Chapter 1. Introduction

1.1. Surface-Enhanced Raman Scattering (SERS)

1.1.1. Raman Spectroscopy

Raman spectroscopy is an analytical technique to observe mainly vibrational and rotational modes of molecules which can be fingerprints. They provide information about the molecular structure and composition.

When a sample is illuminated by a laser beam, three kinds of scattering come out by the interaction between the light and the sample; Rayleigh scattering, Stokes scattering, anti-Stokes scattering.

The huge majority of scattered photons are unchanged in energy so this scattering, so called Rayleigh scattering, is an elastic. While small fraction of them scattered at wavelength different from that of incident laser light. The scattering which turned to lower or higher energy than incident photons is Stokes scattering, anti-Stokes scattering respectively. In usual, Stokes scattering is used in Raman spectroscopy because most molecules exist in ground state in room temperature so Stokes scattering is more intense than anti-Stokes scattering. (see Figure 1)

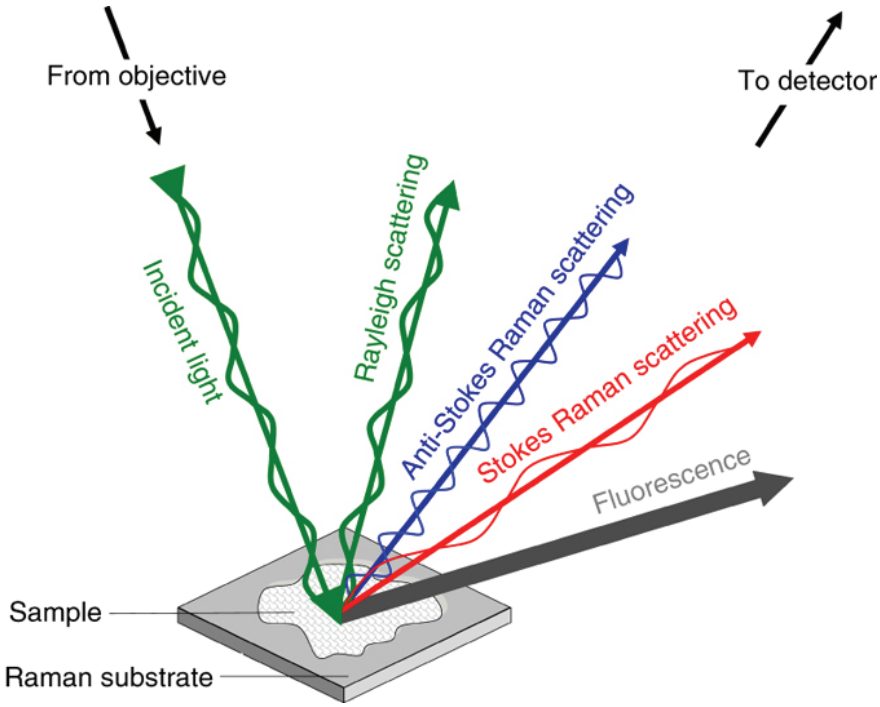

Figure 1. Schematic identifying light scattering after laser exposure on a sample surface.[1]

Compared with infrared spectroscopy, affected by strong water band, Raman spectroscopy can analyze various biomolecules like proteins, carbohydrates, phosphate groups of DNA because significant regions of the Raman spectrum of bio-specimens belong to 400-2000 cm^{-1} wavenumbers.[1]

Still Raman signals inherently is too weak to widely use so it is necessary to enhance Raman signals.

1.1.2. Surface-Enhanced Raman Scattering

Despite benefits of Raman spectroscopy, it was not commonly used due to poor signal to noise ratio. But Raman intensities can be enormously enhanced by two mechanisms. First, rough surface consisted of metal nanoparticles (NPs) shows high enhancement of Raman signals. This phenomenon, called electromagnetic mechanism (EM), is attributed to amplification of the light by the excitation of localized surface plasmons and it leads to enhancing the electric field of the light incident on the molecules. Because laser light can excite electrons in conduction band of metal particles and of these metal NPs silver and gold NPs, especially, have plasmon peaks in visible regions.[2] So they have been widely exploited as plasmonic materials for signal enhancement. EM is widely accepted as main mechanism for SERS. Especially this phenomenon effectively occurs in crevices between metal nanoparticles, so called "hotspot". Thus controlling the hotspots is the key to enhance effectively Raman signals and to study advanced SERS.

The other one is the chemical enhancement (CM), which is related the electronic charge transfer states of molecules and metal NPs. Theoretically the enhancement factor from the chemical can be up to 10^3 whereas the electromagnetic enhancement factor is calculated to ~10^{11}.[3] For the this reason, the effective enhancement

in Raman intensities involves the highly optimized surface that provides electromagnetic field strongly correlated with the wavelength of the light.

1.1.3. Applications of SERS

With enhancing Raman intensities, SERS has been used in various fields including biochemistry, polymer, sensing, material science and catalysis because it allows non-destructive, quantitative and high spatial resolution acquisition. Particularly owing to signal enhancement by SERS, analysis of fragile samples can be available by reduced laser power. Additionally, compared to singe molecule fluorescence that have sample bleaching and richer, single molecule SERS (SMSERS) provides better information. So SERS has been widely used in bio-application fields.

1.1.3.1. *In Vivo* Applications of SERS

In 2006, the first realization of immuno-Raman spectroscopy was performed by by Schlucker et al.[4] They showed the localization of prostate-specific antigen in epithelial tissue from patients with prostate carcinoma. In 2011, the same group reported a paper about a biocompatible gold nanostars whose applications as SERS labels for imaging of the tumor suppressor p63 in prostate biopsies was performed.[5] (Figure 2 and 3)

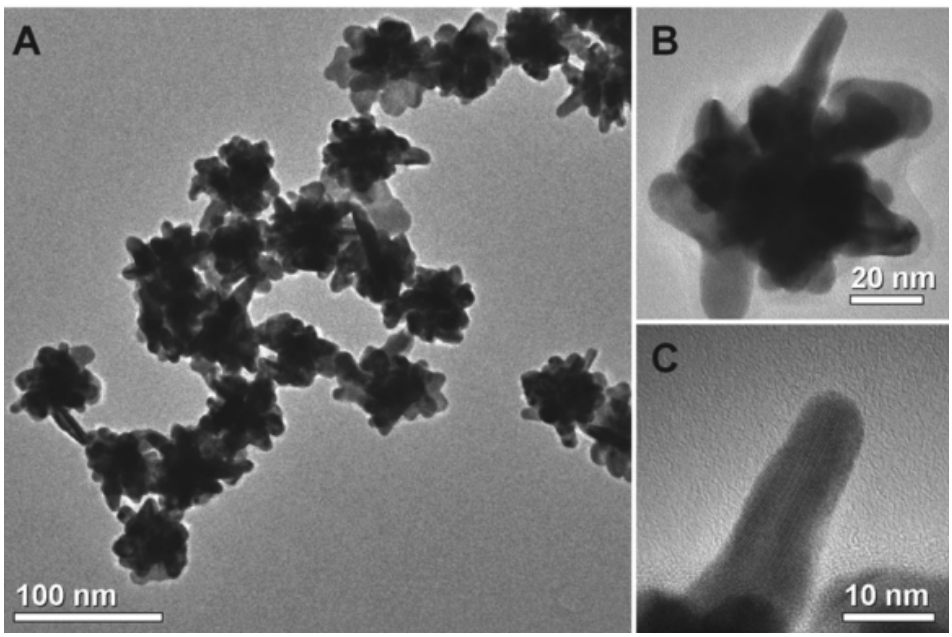

Figure 2. TEM images of B60 nm gold nanostars (A), a single gold nanostar (B) and one of its tips (C) at larger magnification. [5]

In 2008, non-toxic and biocompatible Au NPs for in vivo SERS imaging were described by Qian et al.[6] In this paper, tumors were well targeted with the functionalized gold nanoparticles, which was demonstrated by monitoring SERS signals.[6] (Figure 4)

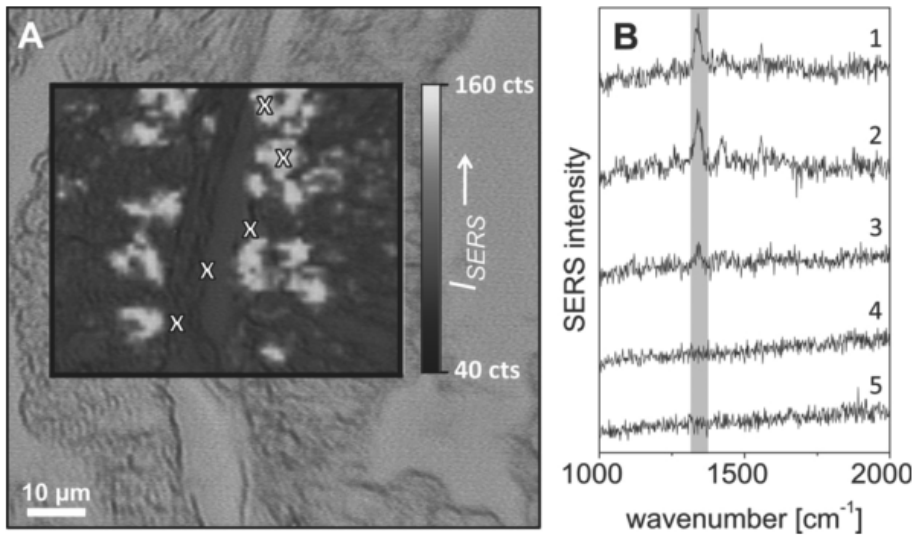

Figure 3. (A) White light image of a prostate tissue specimen with an overlaid SERS false color image based on the intensity of the 1340 cm^{-1} Raman marker band of the SERS label. (B) Five representative SERS spectra from different locations in (A), indicated by white crosses in the SERS false color image (from top to bottom).[5]

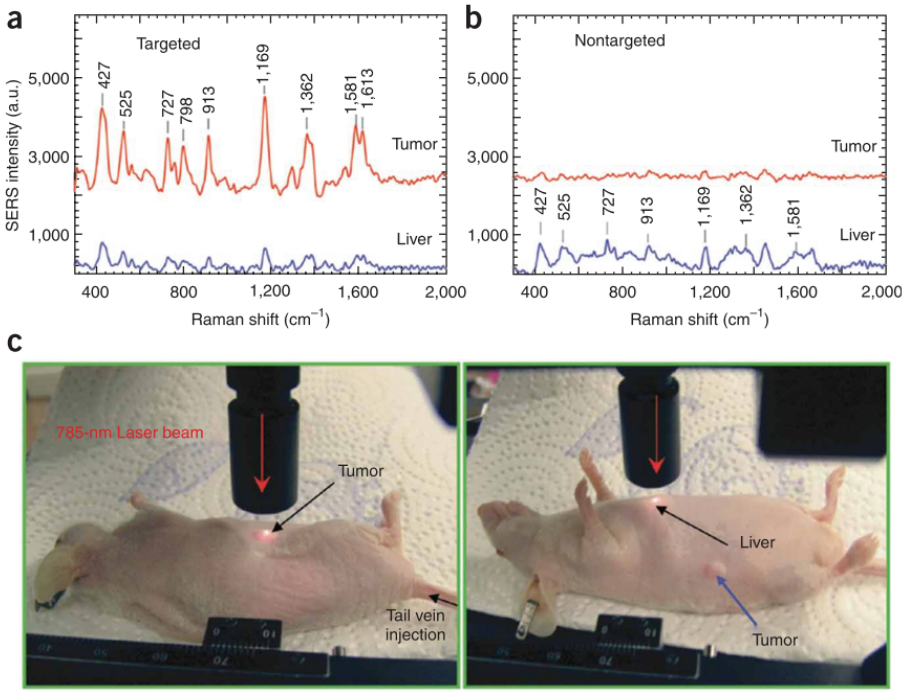
a
Targeted
SERS intensity (a.u.)
5,000
3,000
1,000
427
525
727
798
913
1,169
1,362
1,581
1,613
Tumor
Liver
400
800
1,200
1,600
2,000
Raman shift (cm−1)
b
Nontargeted
5,000
3,000
1,000
Tumor
427
525
727
913
1,169
1,362
1,581
Liver
400
800
1,200
1,600
2,000
Raman shift (cm−1)
c
785-nm Laser beam
Tumor
Tail vein injection
Liver
Tumor

Figure 4. In vivo cancer targeting and surface- enhanced Raman detection by using ScFv- antibody conjugated gold nanoparticles that recognize the tumor biomarker EGFR. (a,b) SERS spectra obtained from the tumor and the liver locations by using targeted (a) and nontargeted (b) nanoparticles. Two nude mice bearing human head-and-neck squamous cell carcinoma (Tu686) xenograft tumor (3-mm diameter) received 90 ml of ScFv EGFR-conjugated SERS tags or pegylated SERS tags (460 pM). The particles were administered via tail vein single injection. SERS spectra were taken 5 h after injection. (c) Photographs showing a laser beam focusing on the tumor site or on the anatomical location of liver. In vivo SERS spectra were obtained from the tumor site (red) and the liver site (blue) with 2-s signal integration and at 785 nm excitation. The spectra were background subtracted and shifted for better visualization. The Raman reporter molecule is malachite green, with distinct spectral signatures as labeled in a and b. [6]

1.1.3.2. *In Vitro* Applications of SERS

There are many *in vitro* applications of SERS technique by using SERS based nanotags which were developed for detection of biomolecules such as glucose[7] or β-amyloid peptide[8]. Recently, functionalized nantags have been studied for disease detection. [9,10](ref) By using gold NPs, the SERS immunoassay platform was fabricated to detect other cancer markers in 2011[9] and nanoparticle-based multiplexed platform that has the potential for simultaneous read-out of pancreatic cancer marker, MUC4 was

developed by Porter et al. in 2013[10] (see Figure 5).

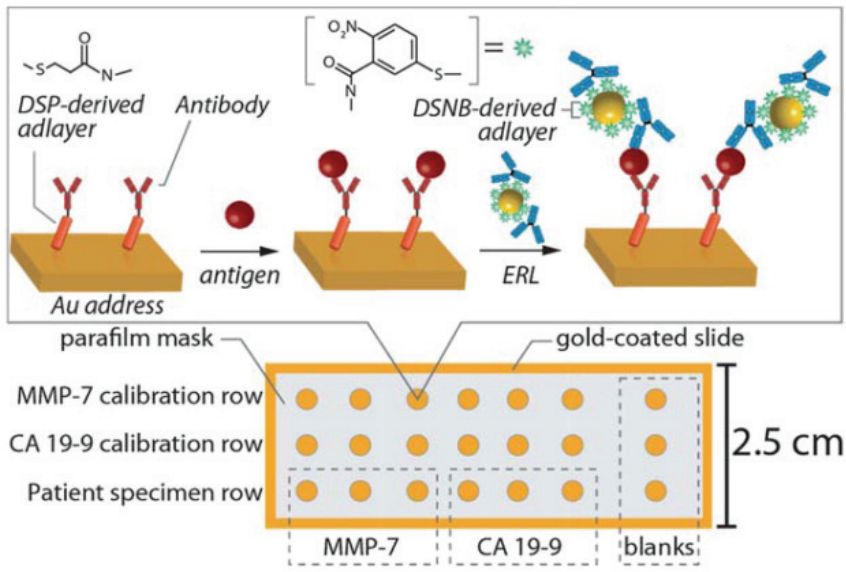

Figure 5. Schematic of SERS array for matrix metalloproteinase-7 (MMP-7) and carbohydrate antigen 19-9 (CA 19-9).[10]

1.1.3.3. Graphene-Enhanced Raman Scattering (GERS)

Beyond traditional SERS, new SERS substrates have been developed for higher enhancement in Raman scattering intensity, good air stability, repeatability, reproducibility and uniformity in signal. For these, graphene and metal oxide NPs are considered promising materials; graphene-enhanced Raman scattering (GERS),[11] metal oxide nanoparticle-enhanced Raman scattering (MONERS).[12]

Graphene is a two dimensional honeycomb structure, consisted sp^2– bonded carbon atoms, and it was discovered in 2004. Due to its notable properties including very high electrical conductivity, inherent strength, flexibility and thermal conductivity, graphene has generated huge interest in a variety of field.

In 2010, Zhongfan Liu et al. showed enhancement of Raman signal from a graphene substrate. The enhancement arose from charge transfer between graphene and molecules and it results in a chemical enhancement.[11] (see Figure 6)

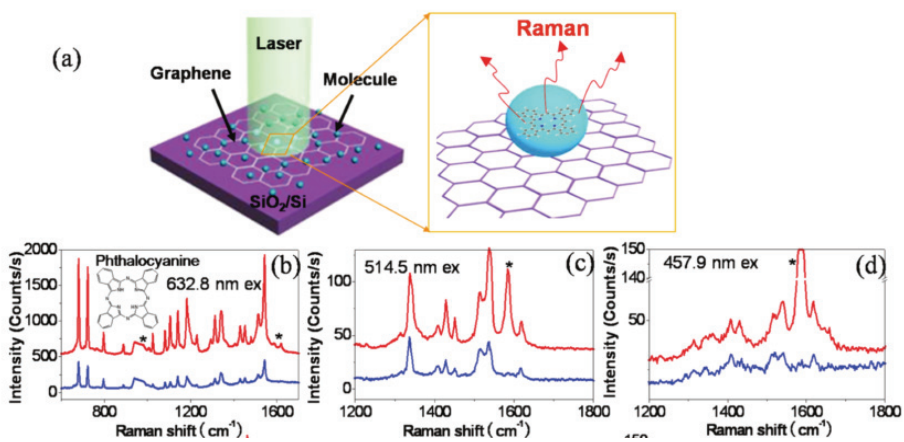

Figure 6. (a) Schematic illustration of the molecules on graphene and a SiO_2/Si substrate, and the Raman experiments. (b–d) are the comparisons of Raman signals of Pc deposited 2 Å on graphene (red line) and on the SiO_2/Si substrate (blue line) using vacuum evaporation at 632.8 nm excitation (b), 514.5 nm excitation (c), and 457.9 nm excitation (d).[11]

1.2. Plasmonic Nanoparticles

1.2.1. Surface Plasmon Resonance

When the light illuminates a metal NP, collective oscillations of free electrons or holes occur and lead to enhanced optical properties like absorption and scattering.[13] Particularly when sizes of NPs are smaller than the wavelength of light, the surface plasmon resonance (SPR) is localized, which is called localized surface plasmon resonance (LSPR).[14] This phenomenon is depicted in Figure 7. Electric fields near the surface of NPs are remarkably enhanced by LSPR. Also the maximum of particle's extinction is located at the plasmon resonant frequency. For a decade, there has been many applied research likes biological(biotin-streptavidin,[15,16] antibody-antigen,[17,18] DNA hybridization[19]) and chemical(gas,[20,21] pH,[22,23] copper[24]) sensor using it.

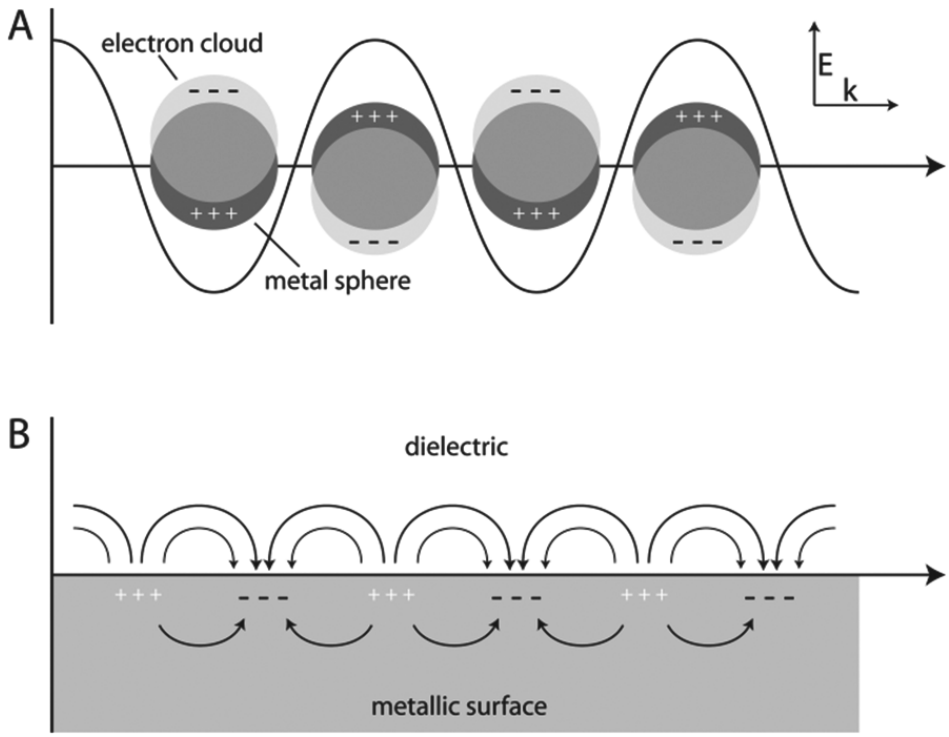

Figure 7. Schematic illustration of (A) localized and (B) propagating surface plasmon polaritons. E depicts the electric field vector and k the wave vector.[25]

1.2.2. Noble Metal Nanoparticles

In the several decades, nanomaterials are consistently studied due to their distinctive optical properties. Especially noble metal NPs such as gold and silver are highly regarded because they have superior oxidation resistance and excitation LSPR by the light NUV, visible, NIR. Also their size and shape are easily controlled so unique, stable and various optical properties can be obtained by using noble metal NPs.[26]

Optical properties of metal NPs are greatly influenced by the LSPR and it depends their size, shape, composition and environment.[27,28] Due to these features, noble metal NPs are considered as key materials in advanced nanotechnology field.

1.2.3. Silver Nanoparticles

As a plasmonic material, silver NPs exhibit optical properties related to surface plasmon resonance. Because silver NPs have strong SPR bands compared with Au NPs, they have been used in fluorescence and SERS.

For several decades, synthetic methods have been developed such as the Turkevich method (citrate synthesis),[29,30] borohydride method,[31] synthesis in two-phase systems,[32] organic reducing agents,[33] synthesis in inverse micelles,[34] laser ablation method,[35] radiolytic methods,[36,37] vacumm evaporation,[38] biosynthesis.[39]

1.2.4. Gold Nanoparticles

Among other nanomaterials Au NPs are widely used due to relatively easy and fast synthetic process. It can be prepared by reducing auric acid with citrate and their sizes can be controlled by adjusting amounts of reagents.

And furthermore their excellent stability and good biocompatibility have made gold NPs be on the list of promising nanomaterials in medical,[40] sensing[41] and therapeutic[42,43] applications.

Chapter 2. Experimental Section

2.1. Materials

The following materials were used as obtained: $AgNO_3$ (Junsei, 99.8%); Sodium citrate tribasic dehydrate (Aldrich, 99%); Sodium borohydride (Aldrich, 99%); (+) Sodium L-ascorbate (Aldrich, 98%); Thiophenol (Aldrich, 99%).

2.2. Size-Controlled Synthesis of Silver Nanoparticles

2.2.1. Preparation of Silver Seeds

The diameter of Ag colloidal particles was controlled by using a seed-mediated process (Figure 8).[44] The Ag seed solution was prepared by mixing 0.30 mL of a 10 mM silver nitrate solution and 20 mL of a 1 mM trisodium citrate solution and then rapidly injecting 1.8 mL of ice-cold 10 mM sodium borohydride. The mixture was then stirred vigorously for 5 min. The resulting solution was aged for 3 h.

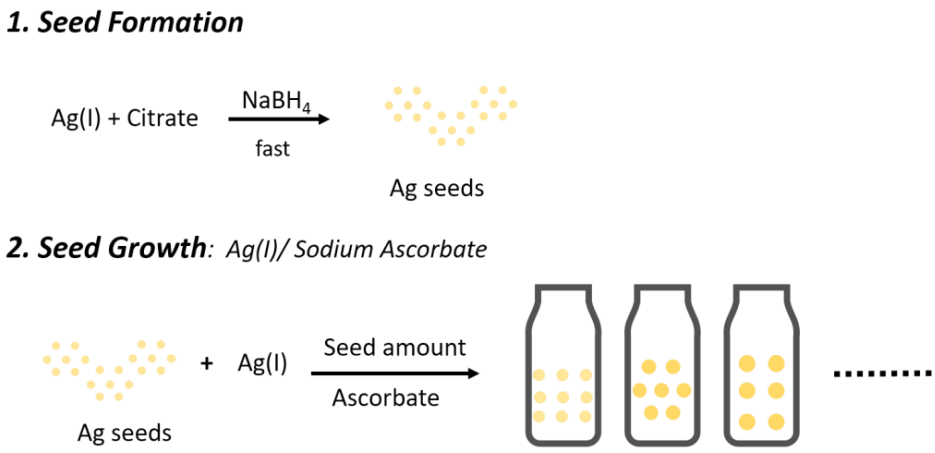

Figure 8. Schematic illustration of preparation of silver nanoparticles.

2.2.2. Seeded Growth of Silver Nanoparticles

The Ag seed solution was aged for 3 h at room temperature. The size of the Ag NPs was controlled by varying the volume of the Ag seed solution relative to the volume of water. X mL of the Ag seed solution, (20 – X) mL of water, and 1.2 mL of a 20 mM sodium ascorbate solution were mixed together. To this solution, 1.2 mL of a 10 mM silver nitrate solution was injected rapidly and then the resulting mixture was stirred vigorously.

2.3. Synthesis of Gold Nanoparticles

2.3.1. Preparation of Gold Seeds

To obtain gold nanoparticles which have various sizes, the seeded growth method based on the classical Turkevich/Frens reaction system was used.[45]

A 15.0 mL volume of aqueous solution containing 2.2 mM sodium citrate was heated at 100 °C with a heating mantle in a two-neck round bottom flask for 30 min. When boiling commences, 0.1 mL of 25 mM $HAuCl_4$ was rapidly added. In about 10 min, the color of the solution changed to bright pink (see Figure 9).

2.3.2. Seeded Growth of Gold Nanoparticles

After reaction was finished, the solution was cooled down to 90 °C and then 0.1 mL of 25 mM $HAuCl_4$ was injected into the flask. This process was repeated at 30 minute intervals.

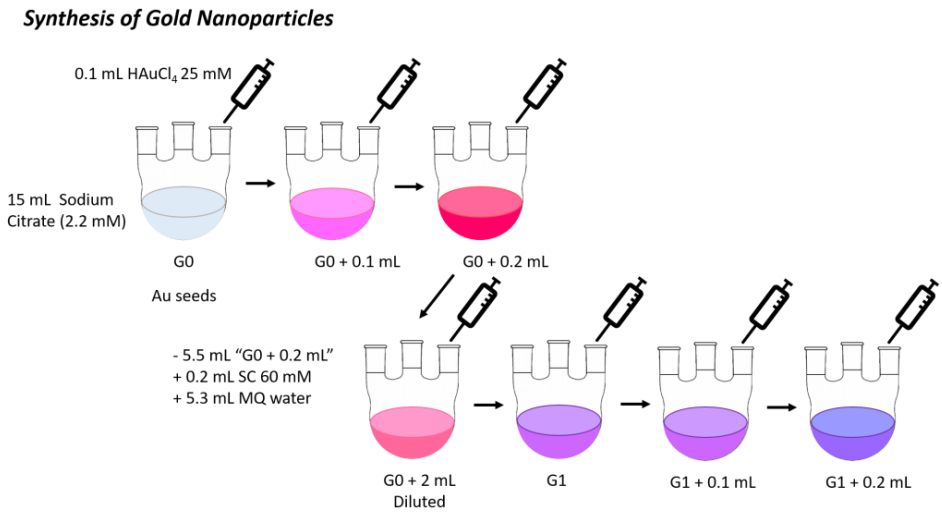

Figure 9. Schematic illustration of the preparation of gold nanoparticles

To remove the ions or salts present in the Ag or Au colloidal solutions, we centrifuged the colloidal solutions at 13,500 rpm for 40 min and removed the supernatant by a pipette. The same volume of distilled water was added to the residue left behind and the resulting mixture was then shaken for 1 min.

2.4. Fabrication of Nanoclusters on a Cover Glass for SERS

P4VP (0.3 g) was dissolved in ethanol (100 mL). 100 μL of this polymer solution was dropped on a cover glass (2.2 cm × 2.2 cm) and the glass plate was rotated at 3,000 rpm for 1 min. The surface of the cover glass was then washed by dipping it in ethanol several

times. The cover glass coated with P4VP was placed in a Petri dish containing a 3.0 mL colloidal solution of Ag or Au to immobilize the colloidal particles on it. After immobilization, the surface was washed with ethanol and then the cover glass was dried by blowing nitrogen gas. To adsorb target molecules on the immobilized colloidal particles, the cover glass was dipped in a 3.0 mL ethanol solution of the target molecules for 24 h. After washing the surface with ethanol, the cover glass was again placed in the Petri dish containing the 3.0 mL colloidal solution of Ag or Au for various durations to immobilize more colloidal particles. The surface of the cover glass was then washed with ethanol and dried. (see Figure 10)

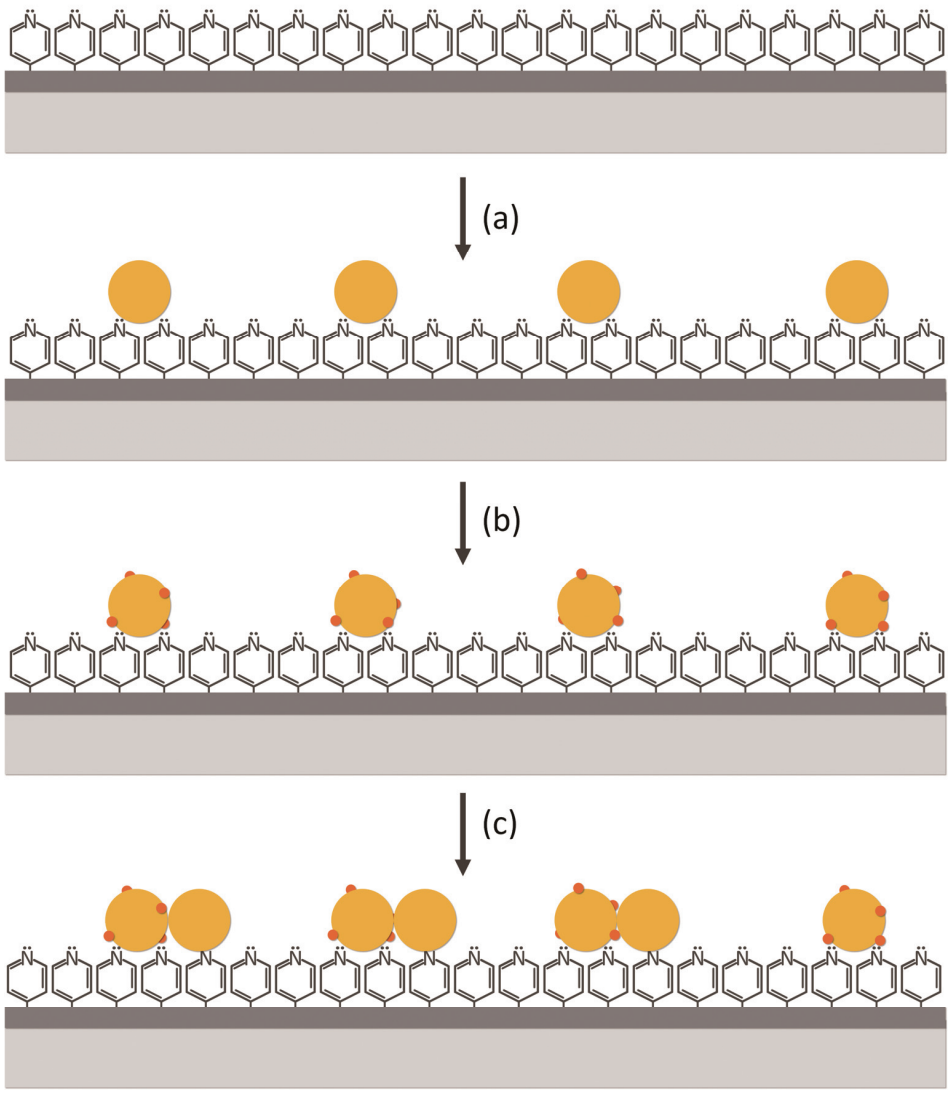

Figure 10. Schematic of the fabrication of SERS substrates consisting of dimers of metal colloidal particles; (a) immobilization of the colloidal particles on a cover glass coated with P4VP, (b) adsorption of target molecules (adsorbates), and (c) second immobilization.

2.5. Characterization

2.5.1. TEM

TEM images of nanoparticles were taken on energy-filtering transmission electron microscope (HR-TEM; JEOL, JEM-3000F) operated with an accelerating voltage of 120 kV.

2.5.2. SEM

The morphology of substrates was checked using a scanning electron microscope (SEM; JEOL ltd. JSM-7800F Prime) operated with an accelerating voltage of 10 kV.

2.5.3. UV-visible Spectroscopy

Extinction spectra were taken using a Double Beam UV-Vis Spectrophotometer (Scinco, Neosys-2000)

The UV-Vis absorption spectra of the colloidal particles immobilized on the cover glass coated with P4VP were obtained by a transmission method. The cover glass coated with P4VP was used as the reference material.

2.5.4. Raman Spectroscopy

Raman spectra were observed by using a micro-Raman system equipped with a homemade sample stage, monochrometer (SPEX 500 M), and CCD camera cooled with liquid nitrogen (Roger

Scientific 7346-001 Model). SERS spectra from the substrates based on Ag NPs were acquired at 514.5 nm, while those from the substrates based on Au NPs at 632.8 nm. The laser power incident on the sample was approximately 10 μW, and acquisition times of 1 and 10 s were used. The Raman spectrum of liquid benzenethiol was obtained from a sample contained in a capillary (364 μm in diameter). Raman frequencies were corrected by using the Raman peaks of a mixture of toluene and acetonitrile (1:1 v/v).

Chapter 3. Dimers of Noble Metal Nanoparticles

Since the advent of surface-enhanced Raman scattering (SERS), researchers have been trying to fabricate highly sensitive and stable SERS substrates. In this chapter, a simple and efficient method to fabricate SERS substrates consisting mainly of Ag or Au dimers by controlling the surface charge of the colloidal particles will be presented. The surface charge was controlled from the pristine colloidal solutions by centrifuging. The SERS substrates were fabricated by a three-step immobilization method as follows: immobilization of colloidal particles, adsorption of target molecules on the immobilized colloidal particles, and second immobilization. The substrates showed very good SERS spectra. For the SERS substrates based on Ag sols, the average enhancement factor was calculated to be ~6.1×10^7.

3.1. Results and Discussion

3.1.1. Synthesis and Characterization of the Noble Metal NPs

Silver and gold colloidal particles were easily synthesized via the seeded growth method. Also the diameters of the spherical Ag and Au NPs were controlled by varying the amounts of seeds and adjusting the growth step. Namely the sizes of NPs are determined by ratio between metal atoms on the surface seeds and added metal atoms. The morphological and optical analysis of Ag NPs having different sizes was performed using a SEM and a UV-vis

spectrophotometer, respectively. The SEM images and extinction spectra of Ag NPs and seeds are shown in Figure 11. As can be seen Figure 11 a-d, As the volume of Ag seeds is increase, the diameter of Ag NPs is decrease. With the size increasing, the position of the LSPR of Ag NPs was red-shifted gradually. Compared with NPs, seeds have broad size distribution and the extinction maximum was located at 390 nm. Because the Ag seeds are too unstable to be grown, it is demanded that Ag seeds be aged for 3 hr. While Ag NPs were capped by citrate, as a stabilizer, they are relatively stable.

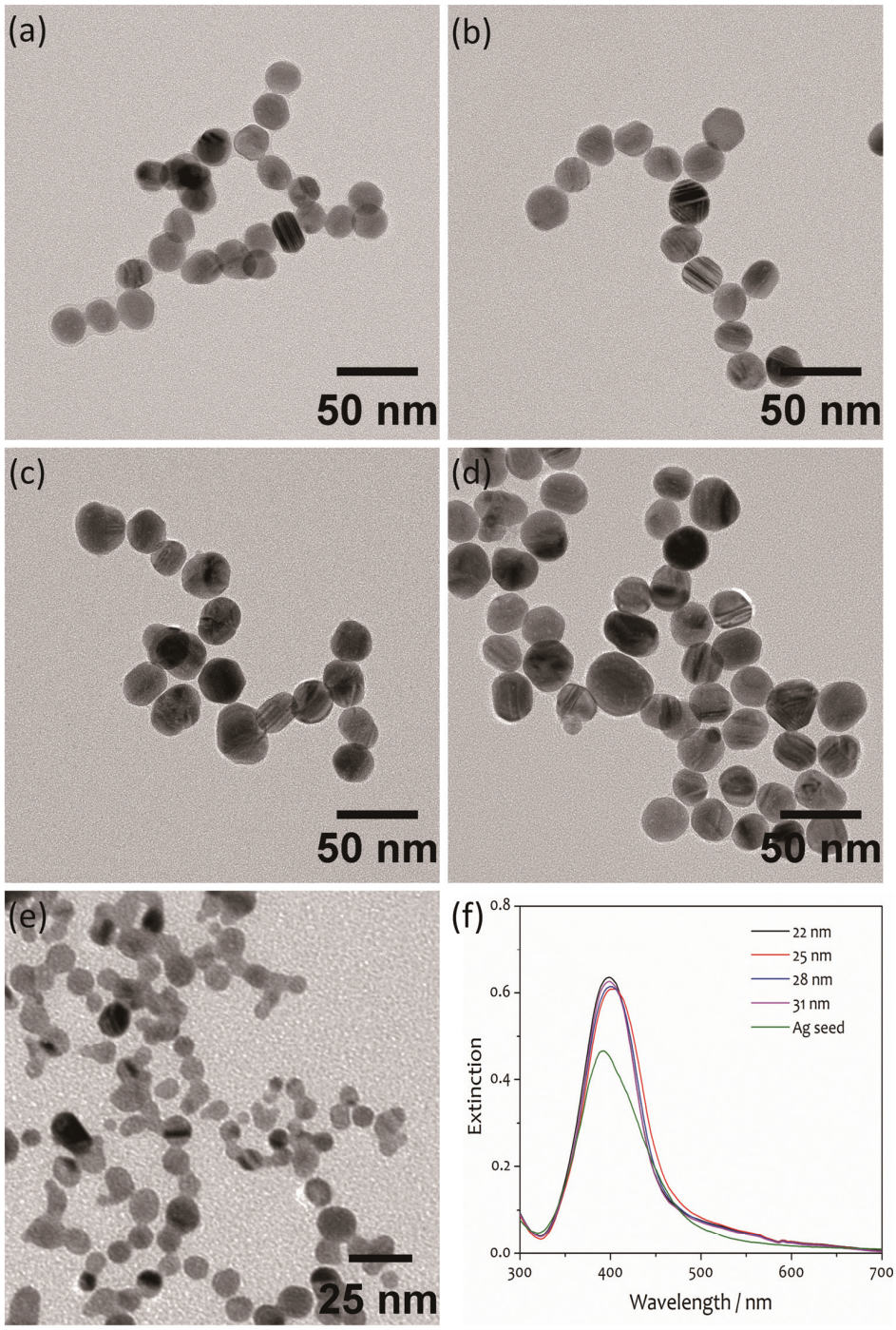

Figure 11. (a–e) SEM images and (f) extinction spectra of Ag (a–d) NPs and (f) seeds.

As the silver nanoparticles, Au NPs were simply synthesized by the seeded growth method and large particles could be easily obtained by repeating the process of growth. As can be seen in Figure 12, the Au NPs have the LSPR band at 522, 528, 534, and 539nm, which longer than those of Ag NPs. From Figure 13, it is possible to identify the shape and size distribution of the Au NPs.

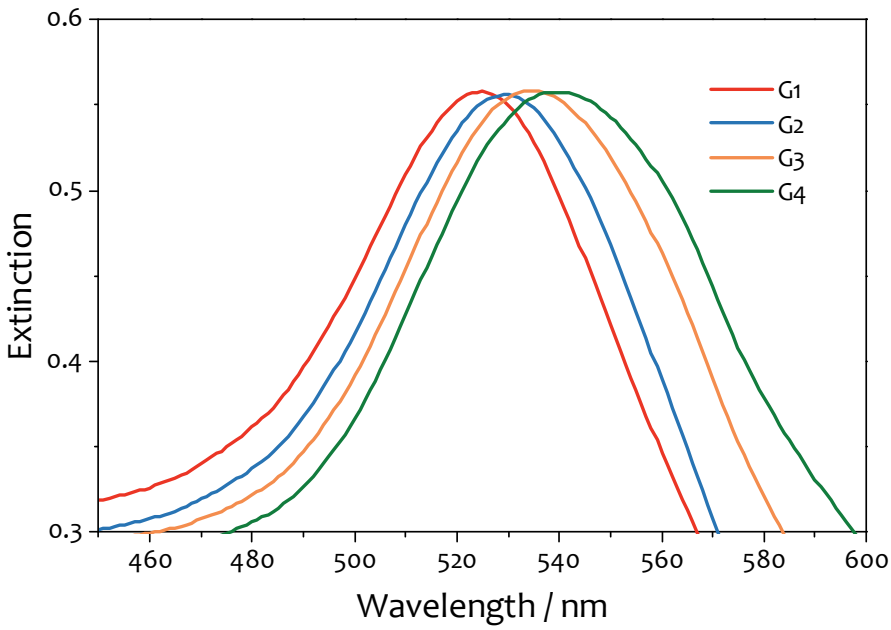

Figure 12. Normalized extinction spectra of Au NPs. The legend shows growth step.

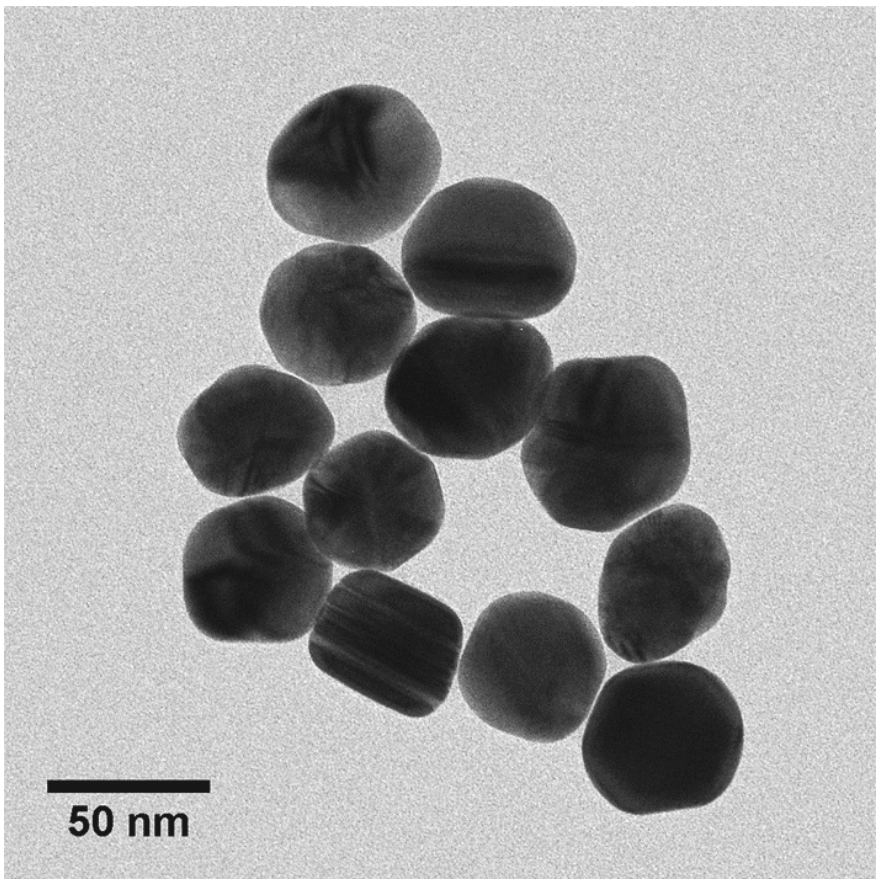

Figure 13. TEM image of Au NPs after 2nd growth step. The average diameter of Au NPs is about 50 nm.

3.1.2. Fabrication of Dimers of Metal Colloidal Particles

To immobilize the Ag or Au NPs onto a cover glass, poly(4-vinylpyridine) (P4VP) was used as a surface modifier. Due to its strong affinity of pyridyl group to metal, the Ag or Au NPs can easily immobilize on the surface of cover glass coated with P4VP. [46] Figure 14 shows the SEM images measured from the substrates fabricated from purified silver sols by using the three-step

immobilization technique and the histogram of the number of Ag colloidal clusters counted from the SEM images. The Ag colloidal particles (28 nm in average diameter) were first immobilized for 10 min on a cover glass coated with P4VP. Benzenethiol was then adsorbed on the immobilized particles and finally, the Ag colloidal particles were immobilized again for various durations. Purified silver sols were prepared by removing the supernatant obtained after centrifuging pristine silver sols, and then adding the same volume of distilled water to the residue left behind. After the purification, the ions present in the pristine silver sols were largely removed, and the surface charge of the Ag colloidal particles was increased significantly. When silver sols purified were used in the immobilizations, all the colloidal particles were immobilized individually, without forming any dimers, during the first immobilization (see Figure 14a). During the second immobilization, dimers of Ag colloidal particles were formed dominantly with very few trimers (see Figure 14b–d). In the SEM images, we can see that the two colloidal particles composing each dimer are in contact with each other. In some cases, they appear to be overlapping. With an increase in the second immobilization duration, the number of dimers increased but not linearly. The histogram of the number of Ag colloidal clusters counted from the SEM images is shown in Figure 14e. The percentage of dimerization was about 65, 73, and 77% when the second immobilization time was 10, 20, and 30 min, respectively. The percentage of dimerization was calculated by

dividing the number of dimers by the number of colloidal particles immobilized during the first immobilization since some colloidal particles could be adsorbed individually even during the second immobilization. It should be mentioned that the second immobilization duration was longer than 40 min, trimers or larger clusters were also formed significantly. This might be caused by increasing the density of immobilized colloidal particles. At relatively high densities of immobilized colloidal particles, some gaps between immobilized particles were equal to or smaller than the diameter of the colloidal particles. In this case, trimers and other larger clusters could be formed by adsorbing new colloidal particles between them. Therefore, it is very important to optimize the first and second immobilization durations to maximize the density of dimers.

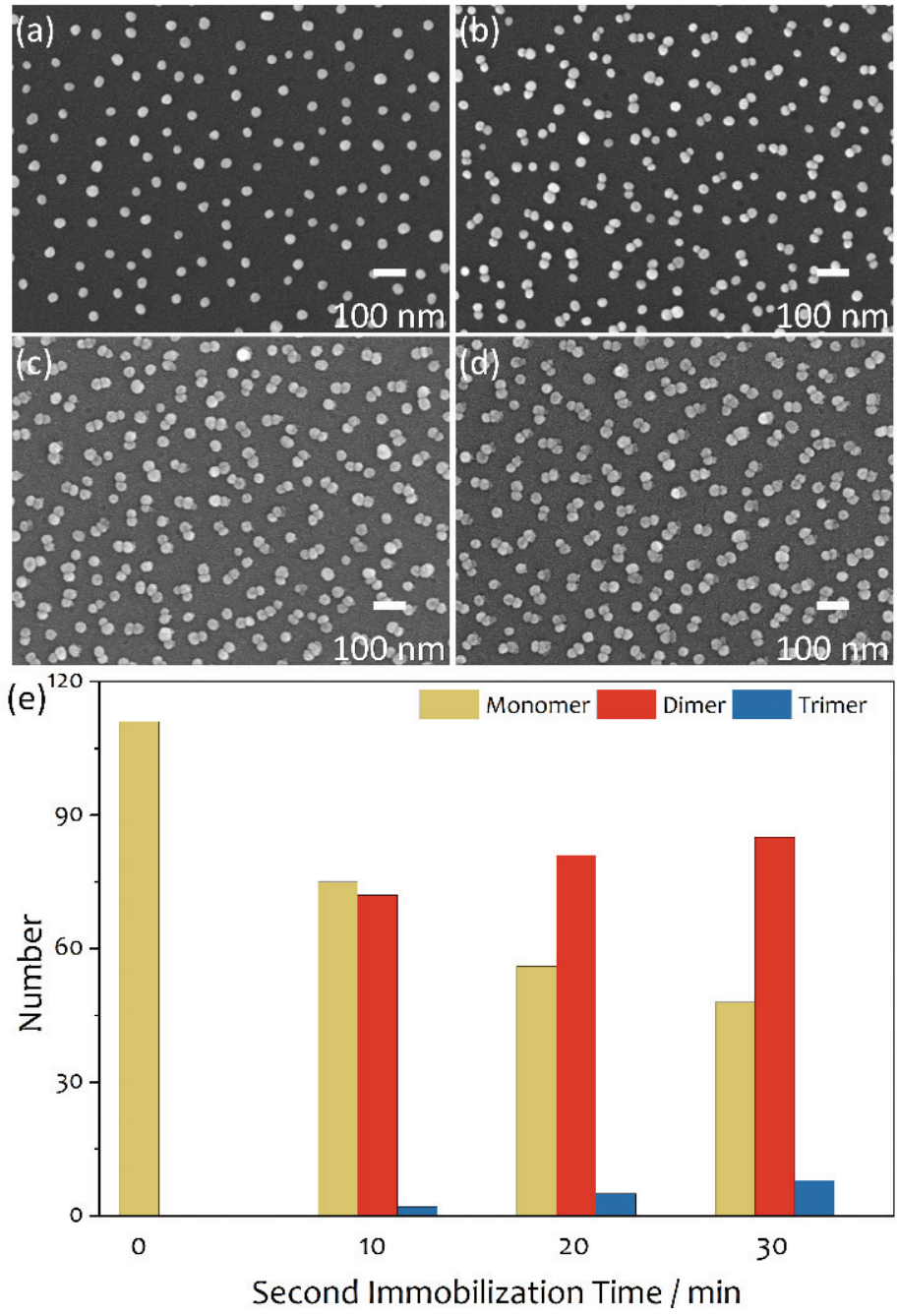
(a)
100 nm
(b)
100 nm
(c)
100 nm
(d)
100 nm
(e)
Monomer
Dimer
Trimer
Number
120
90
60
30
0
0
10
20
30
Second Immobilization Time / min

Figure 14. (a–d) SEM images of the substrates fabricated from purified silver sols by the three-step immobilization process with various second immobilization times and (e) histogram of the number of Ag colloidal clusters counted from the SEM images. The first immobilization time was all the same as 10 min and the second immobilization times were (a) 0, (b) 10, (c) 20, and (d) 30 min. The total amount of benzenethiol adsorbed was all the same for all substrates. The average diameter of the immobilized Ag colloidal particles was about 28 nm.

Ag colloidal particles have the same kind of surface charge, and hence repel each other. When molecules are adsorbed on Ag colloidal particles, the surface charge is altered. Consequently, the force of repulsion between the colloidal particles is reduced. This can result in the aggregation of colloidal particles. It should be noted that for the fabrication of the Ag colloidal particles used in this study, silver nitrate and sodium citrate were added as the reagent and stabilizer, respectively. In addition, sodium borohydride and sodium ascorbate were added as the reducing agents. Therefore, the Ag colloidal particles were surrounded by the ions present in the colloidal solutions such as nitrate, citrate, borate, sodium, etc., and their surface charge reduced significantly. The purification of silver sols reduced the concentration of the ions present in the colloidal solutions significantly. Consequently, the net

surface charge of the colloidal particles increased and the force of repulsion between the colloidal particles increased significantly. With an increase in the force of repulsion between the Ag colloidal particles, the probability of their aggregation during the immobilization decreased. This is the reason why the Ag colloidal particles in the substrate prepared using purified silver sols immobilized individually without any aggregation (Figure 14a). After the adsorption of the target molecules, dimers were formed (see Figure 14b-d). This means that the surface charge of the immobilized Ag colloidal particles was reduced by the adsorption of the target molecules on them. However, it is predictable that the surface charge reduced by adsorption of target molecules increases slightly when dimers are formed by the attachment of fresh colloidal particles. The Ag colloidal particles in the purified silver sols had a relatively higher surface charge than those in the pristine sols. Therefore, it can be expected that the dimers formed from the purified colloidal particles had a higher surface charge than those formed from the pristine ones. It is believed that the dimers formed from the purified colloidal particles had surface charge densities high enough prevent the attachment of new purified colloidal particles to them. Hence, very few larger clusters (trimers and tetramers) were formed.

Figure 15 shows the UV-Vis extinction spectra and benzenethiol SERS spectra measured from the substrates fabricated under the

same conditions as used in the fabrication of the substrates for Figure 14. In the extinction spectra, the Ag colloidal particles immobilized in isolation showed a single LSPR peak at 390 nm, while the dimers of Ag colloidal particles showed two LSPR peaks at 380 and 519 nm. For the dimers, the former peak is attributed to the transverse mode, while the latter is attributed to the longitudinal mode.[47] With an increase in the second immobilization time, the intensity of both the peaks increased without any shift in their extinction peak wavelengths (λ_{max}). The SERS spectra were relatively very strong and well characterized. The SERS peaks observed from the SERS spectra correspond to the modes of the benzene ring of benzenethiol.[48] For example, the peak at 1000 cm^{-1} corresponds to ν_{12}, while that at 1573 cm^{-1} corresponds to ν_{8a}. The peak at 417 cm^{-1} corresponds to ν_{7a} and contributions from the C–S stretching vibration (ν_{CS}). It should be noted that no peaks corresponding to P4VP were observed. The SERS intensity increased with an increase in the number of dimers but decreased significantly when larger clusters like trimers and tetramers were formed at longer second immobilization times. The standard deviation of relative intensities measured at 10 different points of each sample was less than 5% when a laser beam with a diameter of ~1 μm was used. (See Figure 16 and Table 1)

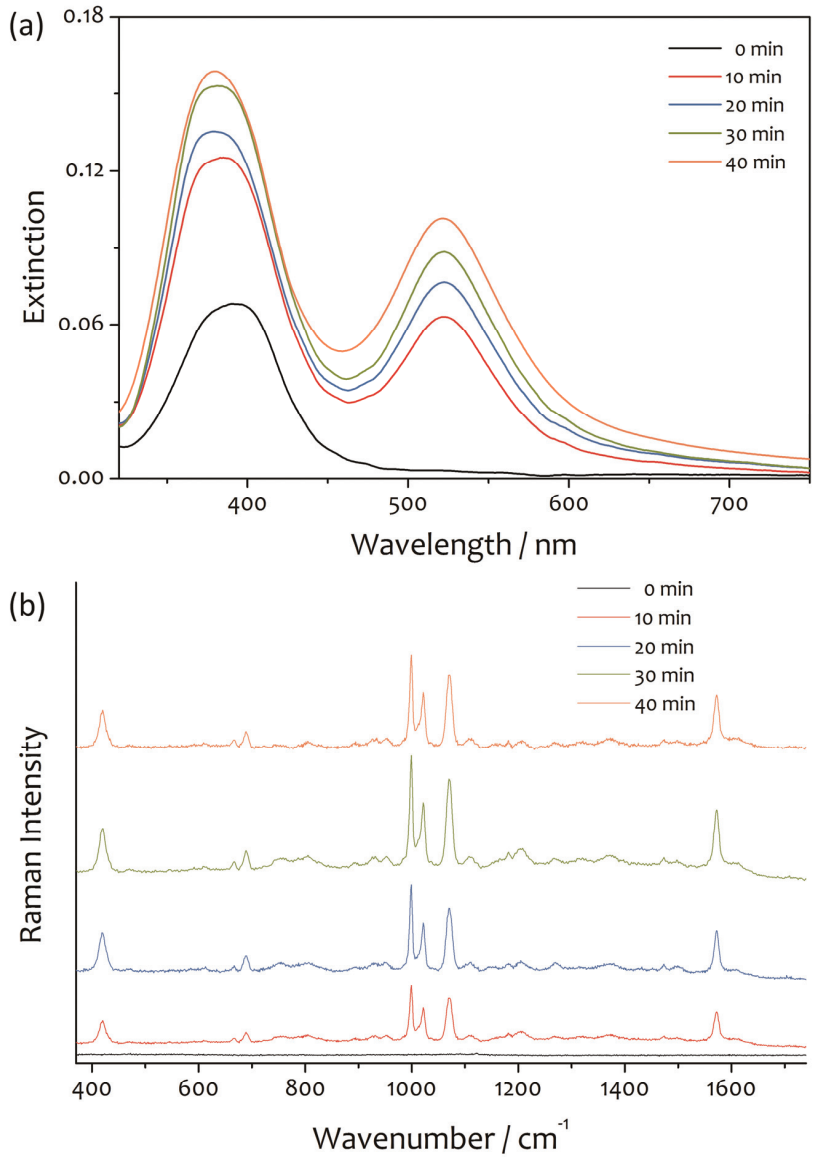

Figure 15. (a) UV-Vis extinction spectra and (b) benzenethiol SERS spectra measured from the substrates fabricated under the same conditions as used in the fabrication of the substrates for Figure 1. The legend shows the second immobilization times. A 514.5 nm Ar-ion laser line was used as the excitation source. The acquisition time was 1 s.

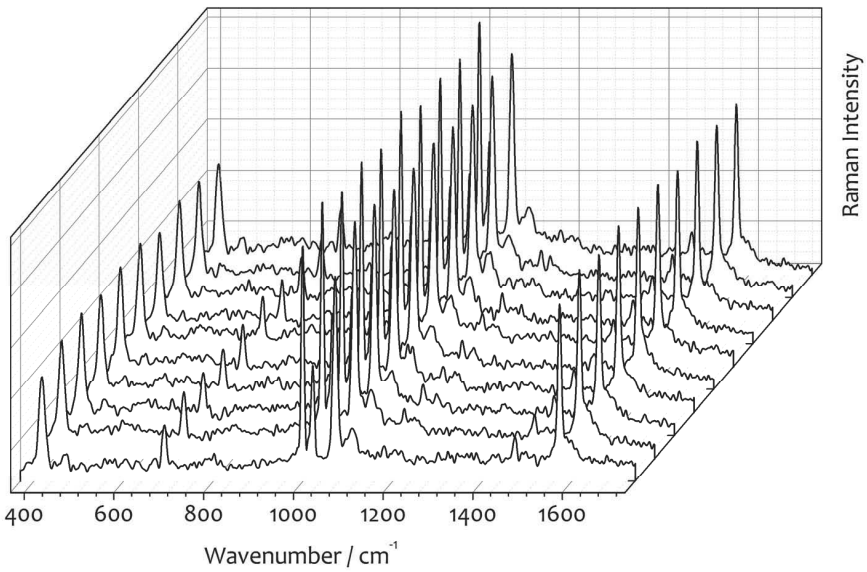

Figure 16. SERS spectra of benzenethiol obtained at 10 randomly selected positions within the substrate prepared by the three-step method. The acquisition time was 1 s.

1	2	3	4	5	6	7	8	9	10	RSD(%)
706	631	665	699	645	675	680	711	645	680	4.05

Table 1. Experimental evaluation of relative standard deviation (RSD) of SERS intensity on the substrates prepared by the three-step method.

For comparison purposes, the SEM images, UV-Vis extinction spectra, and benzenethiol SERS spectra measured from the substrates fabricated from pristine silver sols by the three-step immobilization process with various second immobilization times, and the histogram of the number of Ag colloidal clusters counted from the SEM images were shown in Figure 17. When pristine silver sols were used, not all the colloidal particles were immobilized individually during the first immobilization. Some dimers were also formed. During the second immobilization, relatively large clusters such as trimers and tetramers were also formed along with the dimers. The λ_{max} (519 nm) red-shifted significantly with an increase in the second immobilization duration. These results are significantly different from those obtained from the substrates fabricated from purified silver sols (see Figure 14 and 15). The red-shift is attributed to the formation of a large number of trimers and tetramers. In the histogram, we can see that the number of larger clusters increases with increasing the second immobilization duration. Consequently, the relative SERS intensity was much weak compared to that obtained from the substrates prepared using purified silver sols. The SERS intensity measured from the substrates fabricated from purified silver sols was about 6 times higher than that for pristine, not purified, silver sols. The SERS intensity was decreased when the λ_{max} at 519 nm was red-shifted by formation of larger clusters like trimers and tetramers. The reason for this is discussed below. By comparing the results

shown in Figure 15 and 17, it is concluded that the substrates fabricated from purified silver sols give much better SERS spectra than those fabricated from pristine silver sols.

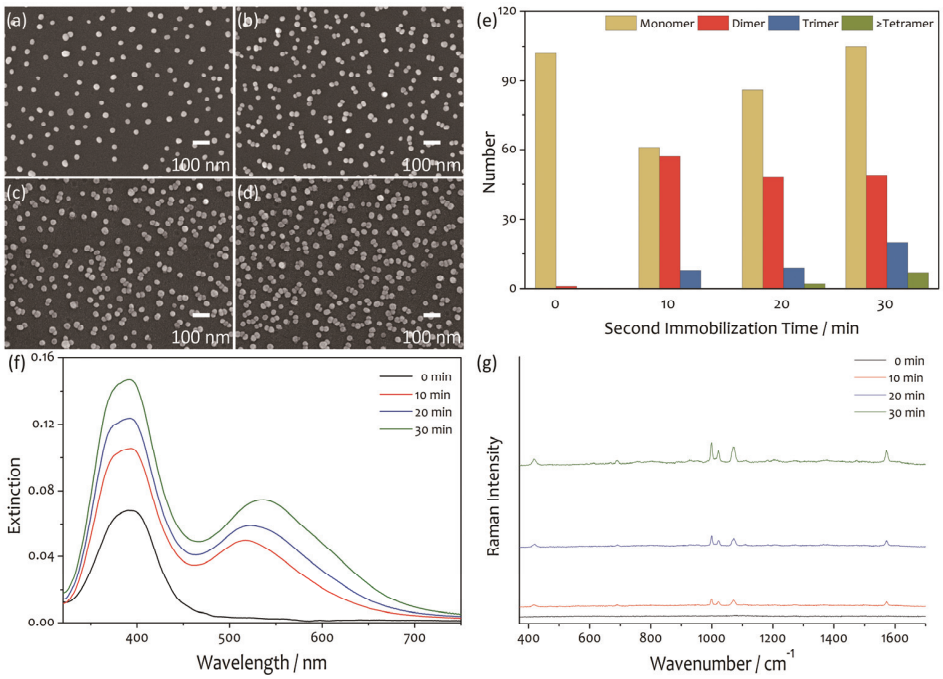

Figure 17. SEM images, UV-Vis extinction spectra, and benzenethiol SERS spectra of the substrates prepared using pristine, not purified, Ag sols by the three-step immobilization process with various second immobilization times, and histogram of the number of Ag colloidal clusters counted from the SEM images. The first immobilization time was 10 min and the second immobilization times were (a) 0, (b) 20, (c) 30, and (d) 60 min. The average diameter of the immobilized Ag colloidal particles was about 28 nm. The legend shows the second immobilization times. A 514.5 nm Ar-ion laser line was used as the excitation source. The acquisition time was 1 s.

The SERS enhancement was calculated by comparing the intensity of the 1575 cm^{-1} peak in the SERS spectrum with that in the normal Raman spectrum. The average enhancement factor for the SERS substrate prepared by the three-step method was calculated to be approximately 6.1×10^7 (chapter 5 covers enhancement calculation). This value is about 60 times higher than the reported one.[47] [It should be mentioned that the reported enhancement was measured from the substrates fabricated by using the three-step immobilization technique. However, pristine silver sols were used in the immobilizations and the diameter of Ag colloidal particles was not optimized.] The average enhancement was affected by the surface concentration of benzenethiol, which was the target molecules. With increasing the concentration, the average enhancement was decreased slowly (see Figure 18). This could be explained by assuming that on the surface of Ag colloid there are some extraordinary sites showing a higher SERS enhancement than others, and these sites are adsorbed slightly preferentially by adsorbates.

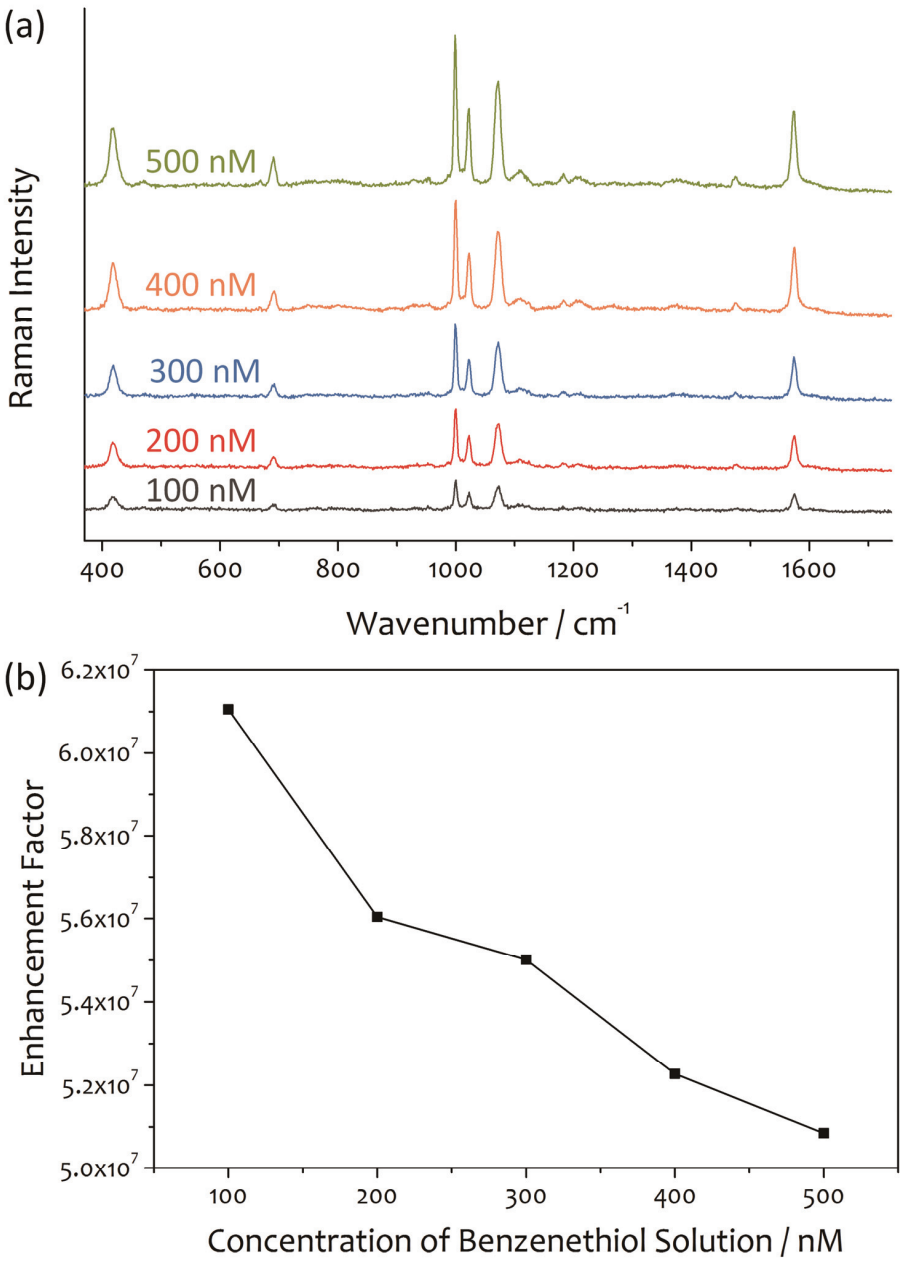

Figure 18. (a) SERS spectra of benzenethiol adsorbed on the substrates at varying concentrations from 50 to 500 nM. (b) Enhancement factors of the substrates as a function of the concentration of benzenethiol solution. The acquisition time was 1 s.

This simple and efficient method to fabricate dimers is applicable to gold NPs as well (see Figure 19). Like silver, gold dimers have sharp extinction spectrum as can be seen in Figure 20.

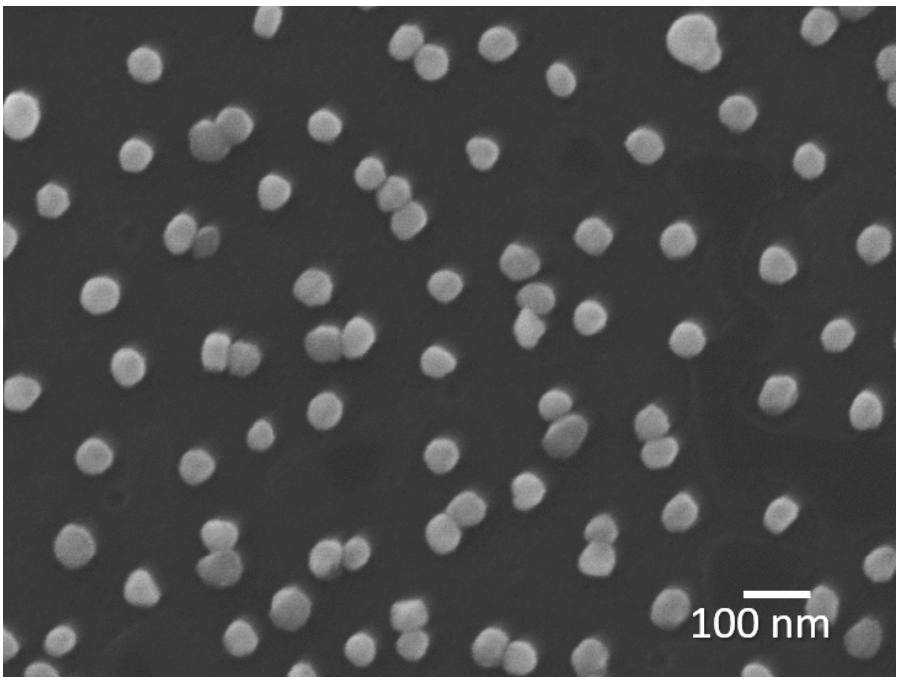

Figure 19. SEM image of Au clusters immobilized on a cover glass coated with P4VP.

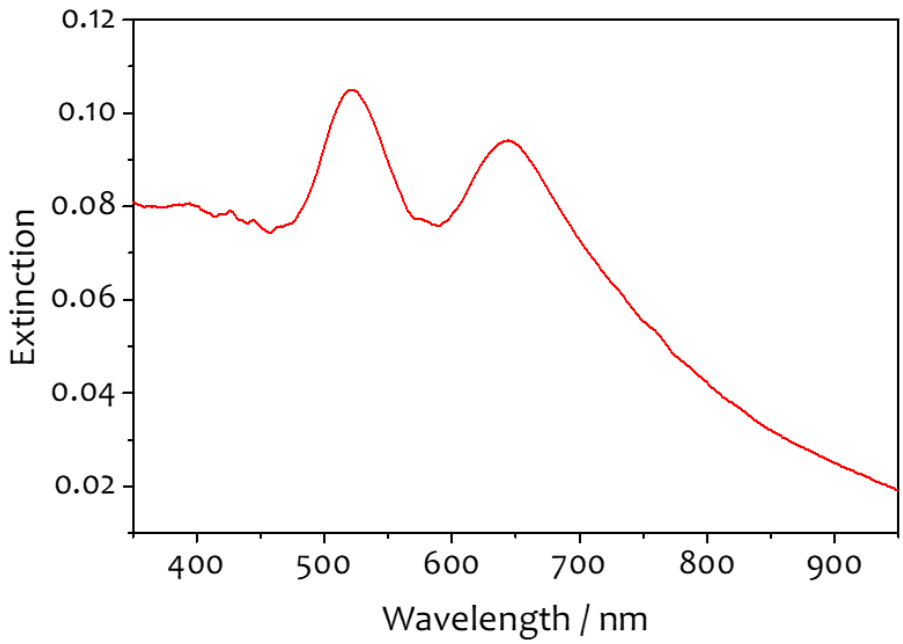

Figure 20. Extinction spectrum of Au dimers immobilized on a cover glass coated with P4VP.

3.2. Conclusions

A simple and efficient three-step immobilization method to preferentially form dimers of metal colloidal particles such as Ag and Au was developed. This method had the following steps: immobilization of colloidal particles on a glass coated with poly(4-vinyl pyridine), adsorption of target molecules on the immobilized colloidal particles, and second immobilization of the colloidal particles. When purified silver sols were used in the immobilizations, dimers of Ag colloidal particles were formed dominantly, with forming very few larger clusters like trimers and tetramers. The

purification of silver sols reduces the concentration of the ions present in the colloidal solutions significantly. Consequently, the net surface charge of the colloidal particles increases and the force of repulsion between the colloidal particles increases significantly. The dimers formed from the purified colloidal particles might have surface charge densities high enough prevent the attachment of new purified colloidal particles to them. Hence, very few larger clusters (trimers and tetramers) could be formed. The fabricated substrates were stable and showed very good SERS spectra. This method could be used to measure SERS spectra of most molecules.

Chapter 4. Effect of Particle Diameter on Surface-Enhanced Raman Scattering

By excitation with a 514.5 nm laser line, the highest enhancement was obtained when the λ_{max} of the longitudinal mode of the dimers of Ag colloidal particles was around 519 nm. The optimum value of λ_{max} was slightly greater than the wavelength of the laser line used. This is because of the fact that the SERS intensity is strongly correlated to the extinction at excitation and Stokes wavelengths. The SERS scattered power can be described as a function of the electro-magnetic field enhancement:[49]

$P_s(\nu_s) = N\sigma_{SERS}|E(\nu_l)|^2|E(\nu_s)|^2 I(\nu_l)$ where $E(\nu_l)$ is the local field enhancement factor at the excitation frequency, while $E(\nu_s)$ is that at Raman scattering frequency; here, N is the number of molecular scatters, σ_{SERS} is the SERS scattering cross-section, and I is the irradiation intensity. When a 514.5-nm laser line is used for excitation, the Stokes Raman scattering wavelength becomes greater than the laser line wavelength by 10–45 nm depending on the modes. Therefore, the SERS intensity reaches the maximum value when λ_{max} of the longitudinal mode of Ag colloidal NP dimers is somewhat greater than the wavelength of the laser line used. The λ_{max} of the longitudinal mode of the dimers red-shifted with an increase in the diameter of the Ag colloidal particles (see Figure 21). The diameter of the Ag colloidal NPs was controlled by using a seed-mediated process[44] (see Figure 22). A λ_{max} of 519 nm was

achieved when dimers were formed from the Ag colloidal particles whose average diameter was 28 nm.

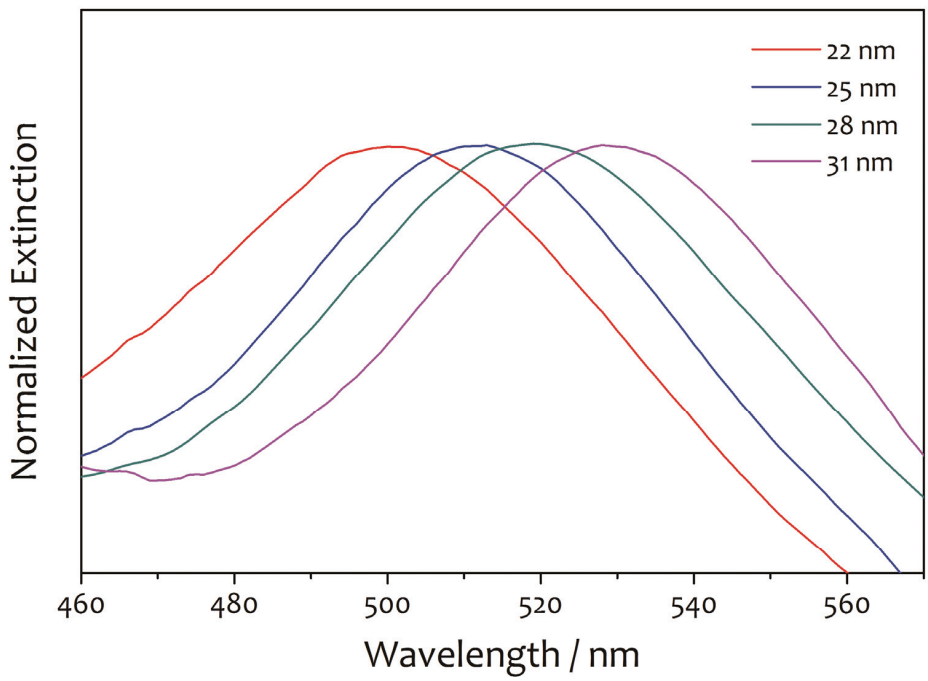

Figure 21. Normalized UV-Vis extinction spectra measured from the substrates prepared by a three-step immobilization technique using purified Ag sols whose average diameter of colloidal particles were 22, 25, 28 and 31 nm. The legend represents the average diameters of Ag colloidal particles.

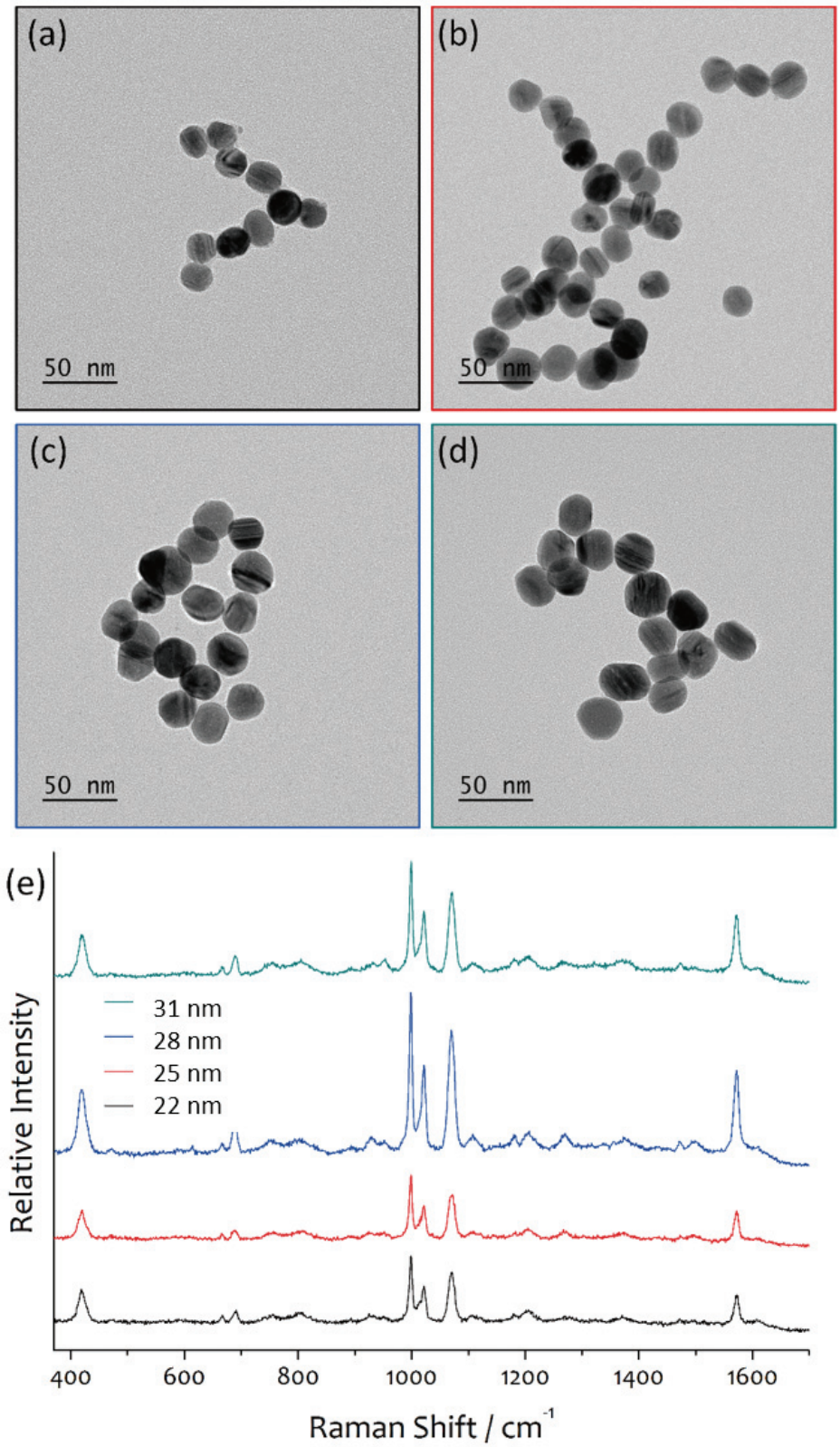
(a)
50 nm
(b)
50 nm
(c)
50 nm
(d)
50 nm
(e)
31 nm
28 nm
25 nm
22 nm
Relative Intensity
400
600
800
1000
1200
1400
1600
Raman Shift / cm-1

Figure 22. (a) UV−vis extinction spectra of the substrates Ag colloidal particles whose average diameters were 22, 25, 28, and 31 nm, and (b) SERS spectra of benzenethiol adsorbed on the substrates prepared by the three−step immobilization technique using four different Ag nanoparticles in average diameter. The acquisition time was 1 s.

Chapter 5. Calculating the Enhancements inside and outside of Ag Dimers

The enhancements inside and outside the junctions of Ag colloidal dimers were experimentally measured. Two kinds of substrates for surface-enhanced Raman scattering were prepared by using three- and four-step immobilization methods. The three-step method consists of following procedures: immobilization of Ag colloidal particles, adsorption of target molecules on the immobilized colloidal particles, and second immobilization. For the four-step method, aniline was adsorbed in the second step, while target molecules in the fourth step. When Ag sols purified by centrifuging were used in the immobilizations, dimers were formed predominantly with forming very few trimers. The substrate fabricated by the three-step method showed 6.5 times higher in SERS intensity than that of the substrate fabricated by the four-step method. In both methods, the dimers were formed during the second immobilization. Therefore, the intensity difference was due to that some target molecules were present at the junctions for the former substrate, while none at the junctions for the latter substrate. From the intensity difference, the enhancements inside and outside the junctions, which acted as hotspots, of the dimers were distinctly calculated. They were 3.5×10^{9} and 1.5×10^{7}, respectively.

5.1. Results and Discussion

Figure 23 shows the SEM image of the substrate after the first immobilization (a), and SEM images of two different SERS substrates prepared by the three-step (b) and four-step (c) immobilization methods. The average diameter of the colloidal particles was about 28 nm, which showed the highest SERS intensity from their dimers (see Figure 22). In the three-step method, Ag colloidal particles were immobilized on a cover glass coated with P4VP, and then benzenethiol as a target molecule was adsorbed on the immobilized particles in the first step, and finally Ag colloidal particles were immobilized again. In the four-step method, Ag colloidal particles were immobilized, and then aniline, instead of benzenethiol, was adsorbed on the immobilized particles, and then Ag colloidal particles were immobilized again, and finally benzenethiol was adsorbed. When target molecules or aniline were adsorbed on the surface of Ag colloidal particles immobilized, the surface charge of the Ag colloidal particles immobilized reduced, and in the second immobilization the repulsion force between the Ag particles immobilized and fresh Ag colloidal particles approaching to them decreased, and the dimerization could take place. In both methods, the first and second immobilization times were the same as 10 and 30 min, respectively. The adsorption times of aniline and benzenethiol molecules were all the same as 24 h. In addition, the total amount of benzenethiol adsorbed on both the SERS substrates fabricated on a cover glass (22 mm × 22 mm) was the same

(3.0×10^{-10} mole). In the immobilizations, silver sols purified by centrifuging were used. The purification of silver sols reduced the concentration of the ions present in the sols significantly. Consequently, the net surface charge of the Ag colloidal particles increased and the force of repulsion between the colloidal particles increased significantly. All the colloidal particles were immobilized individually, without forming any dimers in the first immobilization (see Figure 23a). This is due to the increased surface charge of the purified Ag colloidal particles. In the second immobilization, the dimers of Ag colloidal particles were formed dominantly, while very few trimers were formed (see Figures 23b, c). [In the SEM image (a), there are 117 monomers. In the image (b), there are 75 monomers, 72 dimers and 2 trimers. In the SEM image (c), 74 monomers, 77 dimers, and 2 trimers.] It should be mentioned that when pristine silver sols were used in the immobilizations, not all the colloidal particles were immobilized individually during the first immobilization and relatively large clusters such as trimers and tetramers were also formed along with the dimers during the second immobilization (see Figure 24).

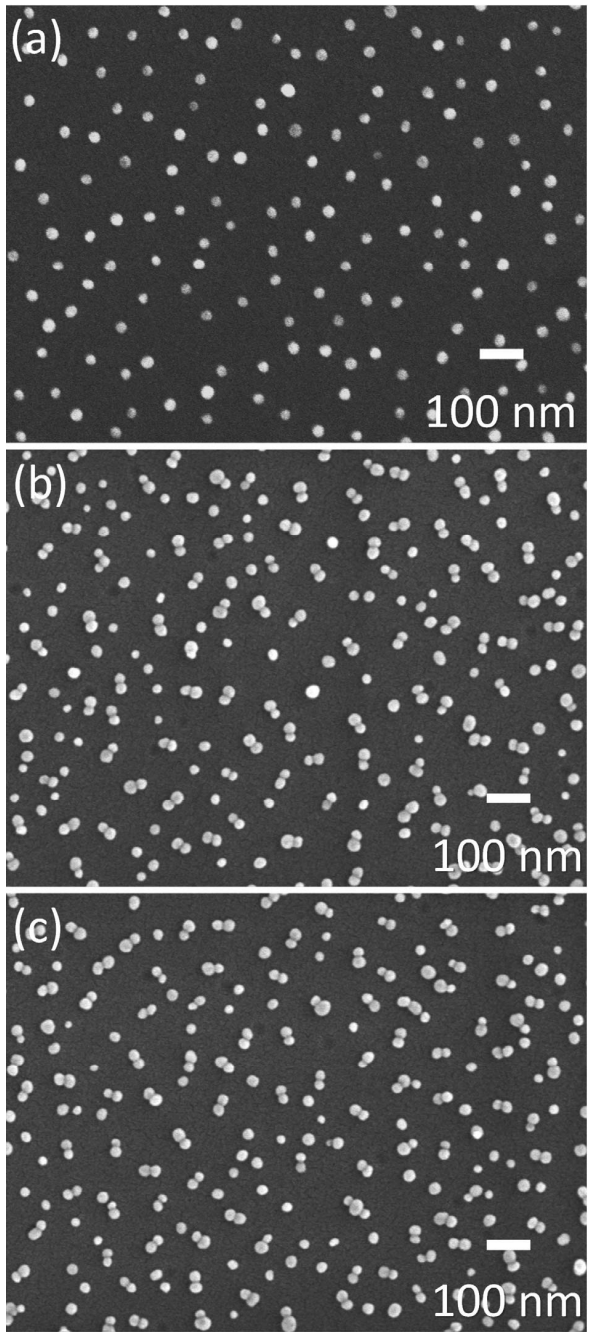
(a)
100 nm
(b)
100 nm
(c)
100 nm

Figure 23. SEM image of the substrate after the first immobilization (a), and SEM images of two different SERS substrates prepared by the three-step (b) and four-step (c) immobilization methods. In both methods, the first and second immobilization times were the same as 10 and 30 min, respectively. The total amount of benzenethiol adsorbed on each substrate was the same. In the SEM image (a); there are 117 monomers. In the image (b); 75 monomers, 72 dimers, and 2 trimers. In the SEM image (c); 74 monomers, 77 dimers, and 2 trimers.

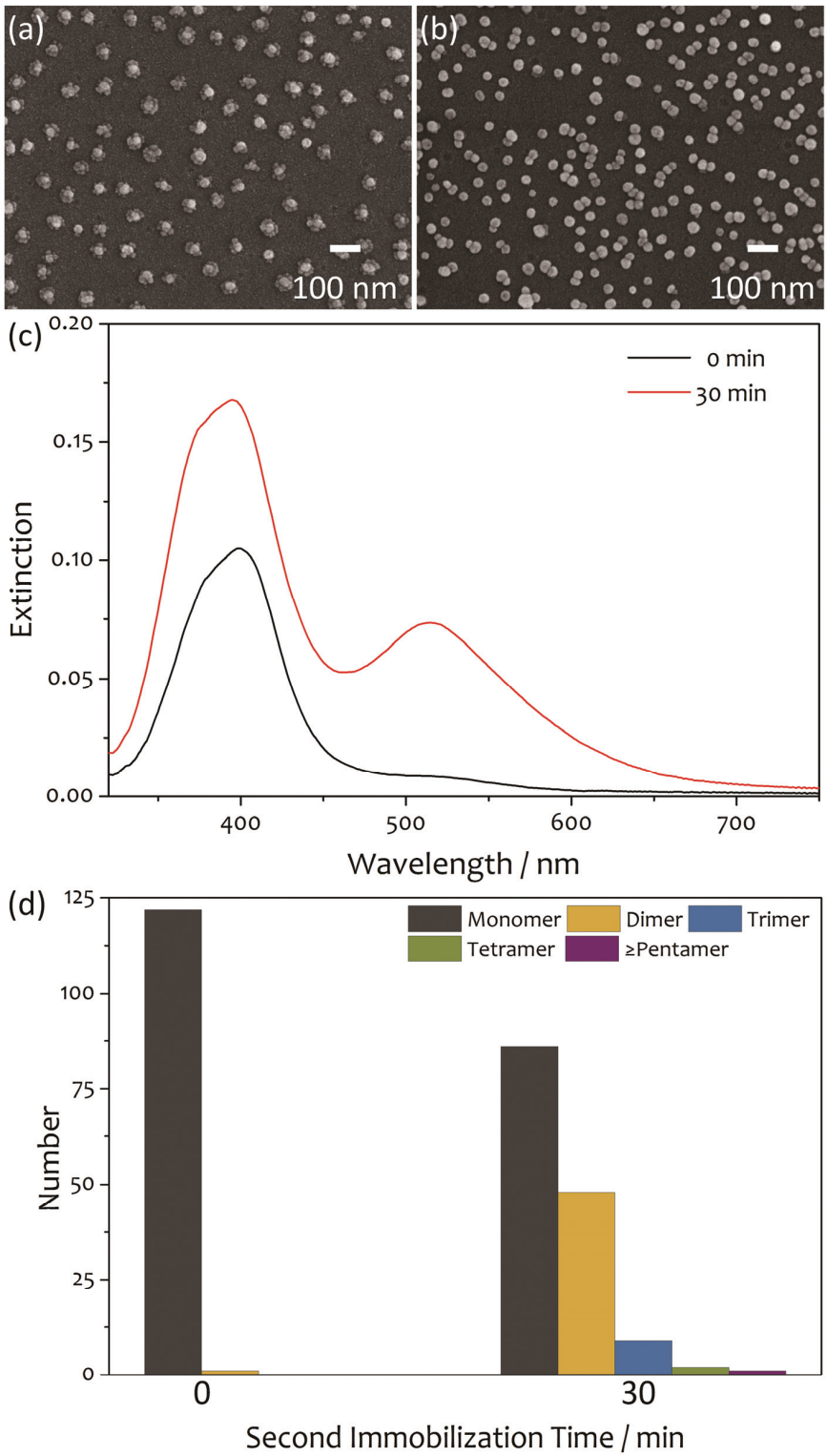
(a)
100 nm
(b)
100 nm
(c)
0 min
30 min
Extinction
0.20
0.15
0.10
0.05
0.00
400
500
600
700
Wavelength / nm
(d)
Monomer
Dimer
Trimer
Tetramer
≥Pentamer
Number
125
100
75
50
25
0
0
30
Second Immobilization Time / min

Figure 24. (a–b) SEM images, (c) UV–Vis extinction spectra, and (d) benzenethiol SERS spectra of the substrates prepared using pristine, not purified, Ag sols by the three–step immobilization process with various second immobilization times, and (d) histogram of the number of Ag colloidal clusters counted from the SEM images. The first and second immobilization times were 10 and 30 min, respectively. The average diameter of the immobilized Ag colloidal particles was about 28 nm. The legend shows the second immobilization times. A 514.5 nm Ar–ion laser line was used as the excitation source.

Figure 25 shows the extinction and SERS spectra measured from the two substrates whose SEM images are shown in Figures 23b and c. The black spectra were measured from the substrate prepared by the three–step immobilization method, while the red ones from the substrate prepared by the four–step method. Both extinction spectra were very similar in terms of the spectral shape and intensity. There are two LSPR peaks at 380 and 519 nm. The former peak is attributed to the transverse mode of the dimers of Ag colloidal particles, while the latter is attributed to the longitudinal mode. Ag colloidal particles immobilized in isolation showed a single LSPR peak at 390 nm (see Figure 15a).

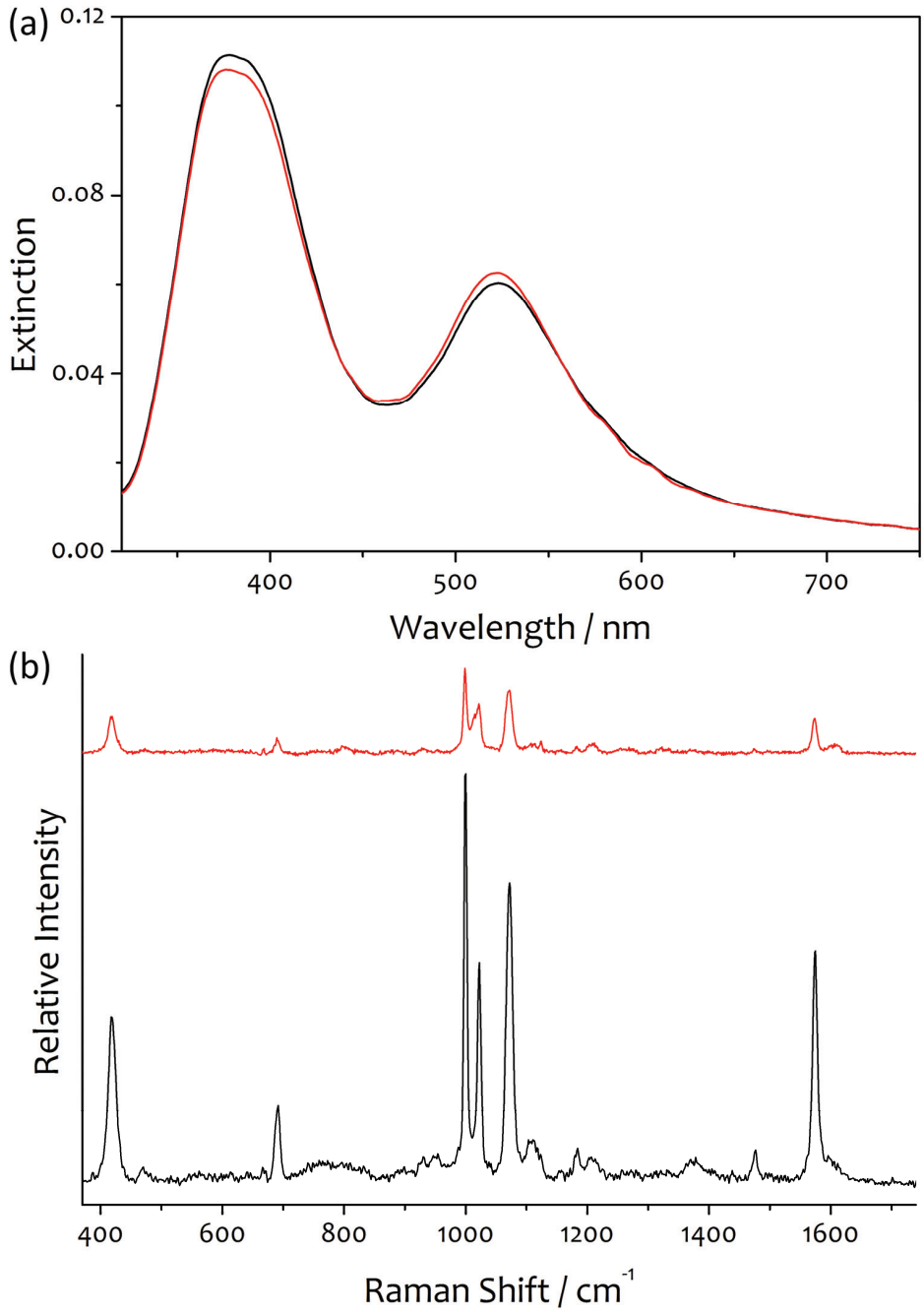
(a)
0.12
0.08
0.04
0.00
Extinction
400
500
600
700
Wavelength / nm
(b)
Relative Intensity
400
600
800
1000
1200
1400
1600
Raman Shift / cm-1

Figure 25. Comparison of (a) UV−Vis extinction and (b) SERS spectra measured from the two different substrates whose SEM images are shown in Figure 23. The black spectra were obtained from the substrate prepared by the three−step method, while the red spectra from the substrate prepared by the four−step method. The total amount of benzenethiol adsorbed on each substrate was the same. The intensity of the black SERS spectrum was approximately 6.5 times stronger than that of the red SERS spectrum. The acquisition time was 1 s and the 50× objective lens was used. For two substrates, the total number of benzenethiol molecules adsorbed was the same and the adsorption time of benzenethiol was also the same as 24 h.

The SERS spectra measured from the two substrates are relatively very strong and well characterized. The SERS peaks observed from the SERS spectra correspond to the modes of the benzene ring of benzenethiol.[48] For example, the peak at 1573 cm^{-1} corresponds to ν_{8a}, while that at 1000 cm^{-1} corresponds to ν_{12}. The peak at 417 cm^{-1} corresponds to ν_{7a} and contributions from the C−S stretching vibration (ν_{CS}). It should be noted that no peaks corresponding to P4VP and aniline were observed. When a 50× objective lens, whose laser beam spot size was ~1 μm in diameter, was used, the standard deviation of relative intensities measured at 10 different points of each sample was less than 5% (see Figure 26 and Table 2). It

should be mentioned that the SERS intensity was just slightly fluctuated, randomly, during measurements of a series of SERS spectra (see Figure 27). This may mean that no laser induced thermal desorption or surface diffusion of benzenethiol molecules took place during measurements. This is due to the fact that benzenethiol is strongly chemisorbed on the silver surface.

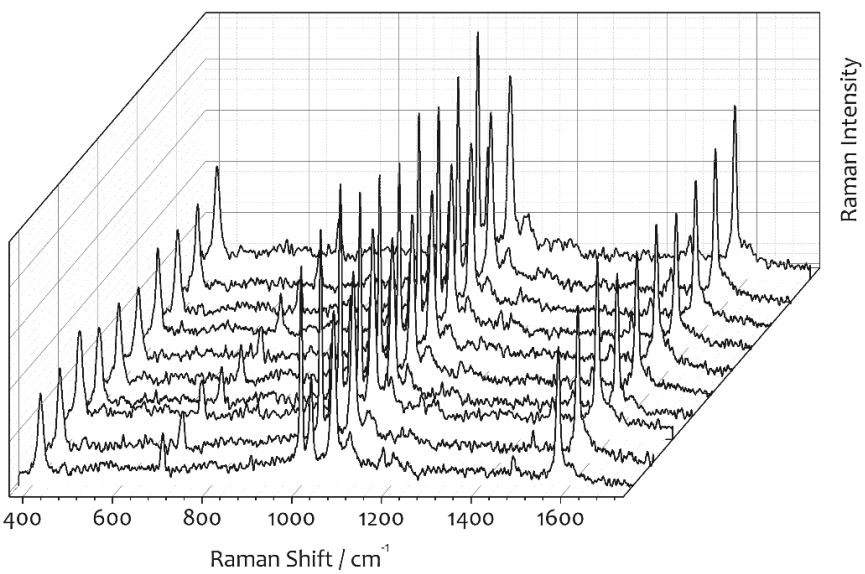

Figure 26. SERS spectra of benzenethiol obtained at 10 randomly selected positions within the substrate prepared by the four-step method. The acquisition time was 1 s.

1	2	3	4	5	6	7	8	9	10	RSD(%)
113	106	103	99	103	102	102	115	107	101	4.92

Table 2. Experimental evaluation of relative standard deviation (RSD) of SERS intensity on the substrates prepared by the four-step method.

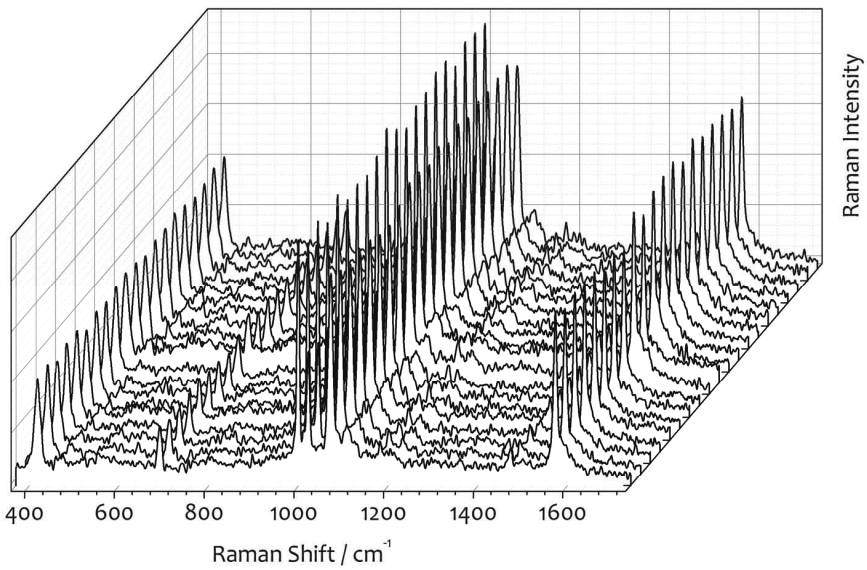

Figure 27. SERS spectra of benzenethiol continuously measured 20 times at intervals of 10 seconds at a position within the substrate prepared by the four-step method. The acquisition time was 1 s.

When the λ_{max} of the longitudinal mode of Ag dimers was around 519 nm, the highest SERS intensity was obtained by excitation with a 514.5 nm laser line. The optimum value of the λ_{max} was somewhat greater than the wavelength of the excitation light. This is owing to the fact that the SERS intensity is strongly correlated to the extinction at excitation and Stokes wavelengths.[50] When a 514.5 nm laser line is used for Raman excitation, the Stokes Raman scattering wavelength becomes greater than the laser line wavelength by 10–45 nm depending on the modes. Therefore, the SERS intensity reaches the maximum value when the λ_{max} is slightly

greater than the wavelength of the excitation light. A λ_{max} of 519 nm was achieved when dimers were formed from 28 nm (average diameter) Ag colloidal particles.

Although their extinction spectra were very similar in terms of the spectral shape and intensity, the SERS intensity measured from the substrate prepared by the three-step method was approximately 6.5 times higher than that measured from the substrate prepared by the four-step method. The LSPR of the monomers of Ag colloidal particles occurs around 390 nm, which is too far to be excited by a 514.5 nm light. Therefore, the SERS signal in these substrates was mainly contributed by the molecules adsorbed on the dimers. Since the transverse mode of the dimers of Ag colloidal particles occurs at 380 nm, which is also too far to be excited by a 514.5 nm light. Therefore, the SERS signals measured by excitation with a 514.5 nm light were mainly contributed by the longitudinal mode of the dimers. [It should be noted that the contribution of the trimers to the observed SERS signals was ignored because the number of the trimers was very few and their longitudinal mode was somewhat apart from the laser line used.] In the three-step method, benzenethiol served as the target molecule and was adsorbed on the Ag colloidal particles immobilized during the first immobilization process. There are 117 individually immobilized Ag colloid particles in the SEM image of Figure 23a, and 72 dimers in the SEM image of Figure 1b. Therefore, the percentage of dimerization among the Ag colloidal particles

immobilized in the first immobilization was about 62% [= 100% × 72/117]. This means that about 62% of benzenethiol molecules were adsorbed on the dimers. [It should be mentioned that some colloidal particles were adsorbed individually even during the second immobilization.] In the four-step method, benzenethiol was adsorbed on the surface of all the colloidal particles of the substrate. Among the total colloidal particles immobilized on the substrate, the percentage of the colloidal particles composing the dimers was found to be about 66% [= 100% × 77×2/(74×1 + 77×2 + 2×3)] (see Figure 23c). This means that about 66% of the benzenethiol molecules were adsorbed on the dimers of the substrate prepared by the four-step method. For the substrate prepared by the three-step method, 62% of target molecules were adsorbed on 72 dimers, while for the substrate prepared by the four-step method 66% of target molecules on 77 dimers. Therefore, each dimer of two substrates had almost the same number of target molecules on its surface [62%/72 ≒ 66%/77 ≒ 0.86%]. Therefore, it can be concluded that the number of benzenethiol molecules adsorbed on each dimer was almost the same in both the substrates.

In the three-step method, benzenethiol was adsorbed on the Ag colloidal particles immobilized during the first immobilization process, and the dimers were formed in the second immobilization process. Therefore, a certain portion of benzenethiol molecules would present at the junctions of the dimers. In the four-step

method, benzenethiol was adsorbed on the surface of all the colloidal particles present on the substrate. However, in order to be adsorbed at the junctions of the already formed dimers, the benzenethiol molecules needed to penetrate into the narrow gap of the junctions between two attached colloidal particles. During the course of diffusion to reach the junctions, the benzenethiol molecules might have collided many times with the surface of the Ag colloidal particles composing the dimers. Since benzenethiol was strongly chemisorbed, it is likely that it was adsorbed on the surface after a few collisions before reaching to the junctions. This means that in the four-step method the benzenethiol molecules could not be adsorbed at the junctions. It should be noted that the spreading of benzenethiol molecules on the surface of the dimers was not the same in the two samples. For the substrates prepared by the three-step method, benzenethiol was adsorbed on the surface of the colloidal particles immobilized in isolation and then the dimers were formed by the attachment of fresh colloidal particles to this assembly. However, for the substrates prepared by the four-step method benzenethiol was adsorbed on the already formed dimers. Therefore, in the substrates formed by the three-step method, benzenethiol was adsorbed on only one particle composing the dimers, while in the substrates formed by the four-step method, it was adsorbed on the both particles composing the dimers. Nevertheless, the SERS intensity would not be affected significantly by this difference. This is because each colloidal

particle composing the dimers in both the substrates may show a similar SERS effect. Therefore, it can be concluded that the difference in the SERS intensity of the two kinds of substrates (Figure 25) resulted from the fact that some benzenethiol molecules existed at the junction regions in the substrates prepared by the three-step method unlike the substrates prepared by the four-step method.

The SERS enhancement was calculated by comparing the intensity of the 1575 cm^{-1} peak in the SERS spectrum with that in the normal Raman spectrum. In calculation of the number of molecules adsorbed on the surface of Ag colloidal particles, it was assumed that all the molecules contained in a 3.0 mL ethanol solution of 100 nM benzenethiol were completely adsorbed on the surface of the colloidal particles immobilized on the cover glass (22 mm × 22 mm). A complete adsorption might be reasonable, since benzenethiol was strongly chemisorbed on silver surface, the adsorption time was long enough as 24 h, and the surface coverage was well below a monolayer. By a simple calculation, the amount of the molecules contained in the 3.0 mL benzenethiol solution was corresponded to about 3.6% of the surface atoms of Ag colloidal particles immobilized during the first immobilization. The average enhancement factor was calculated to be approximately 6.4×10^7 for the SERS substrate prepared by the three-step method (see Figure 28 and the calculation), while 9.8×10^6 for the SERS substrate prepared by the four-step method (see Figure 29 and the

calculation).

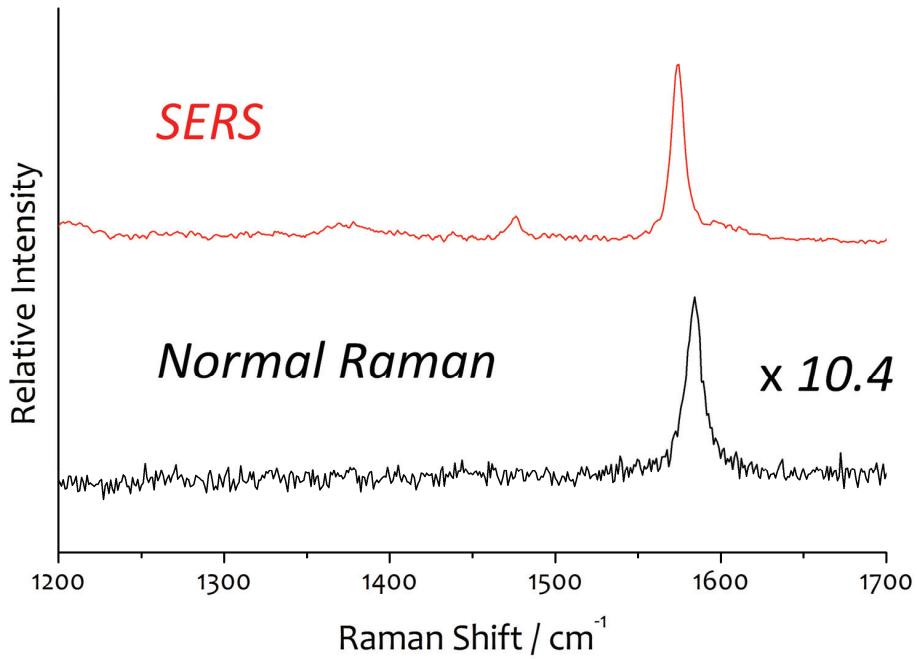

Figure 28. Comparison of the normal Raman spectrum of pure benzenethiol liquid with the SERS spectrum measured from the SERS substrate prepared by the three-step immobilization method. The acquisition time was 1 s. Spectra were acquired at 514.5 nm using a 10× objective (NA = 0.25).

Calculation of the average SERS enhancement measured from the substrate prepared by the three-step method.

The quantity of adsorbed molecules is approximately 3.0×10^{-10} moles [100 nM × 3.0 mL = 100×10^{-9} mole/L × 3×10^{-3} L = 3.0×10^{-10} moles]. The area of the SERS substrate was $4.84cm^2$ [2.2 cm × 2.2 cm]. The number density of adsorbed molecules was

approximately 3.7×10^{5} molecules/μm^2 [3.0×10^{-10} moles × (6.02×10^{23} molecules/mole)/4.84 cm^2 = 3.7×10^{13} molecules/cm^2 = 3.7×10^{5} molecules/μm^2]. The diameter of the laser beam with an objective lens of 10× was approximately 2.5 μm. For SERS measurement, the number of molecules at focused area was 1.8 × 10^6 molecules [= 3.7×10^{5} molecules/μm^2 × 3.14 × (1.25 μm)^2]. A normal Raman spectrum was observed for a 364 μm−thick cell filled with pure benzenethiol liquid that had a density of 1.08 g/cm^3. The molecular mass of benzenethiol is 110 g/mol. The probe volume was approximately 1.8×10^{3} μm^3, calculated by assuming that it is a cylinder with a diameter of 2.5 μm and a height of 364 μm, [3.14 × (1.25 μm)^2 × 364 μm = 1.8×10^{3} μm^3]. Under these conditions, 1.1×10^{13} molecules would be irradiated, [(volume × density × Avogadro's number) / molar mass = 1.8×10^{3} μm^3 × 1.08 g/cm^3 × (6.02×10^{23} molecules/mol)/(110 g/mol) = 1.1×10^{13} molecules]. In Figure 28, the ratio of the SERS intensity to the normal Raman intensity was about 10.4. Therefore, the enhancement factor is calculated to be approximately 6.4×10^{7} [= intensity ratio × (number of molecules irradiated in measuring the normal Raman spectrum)/(that for SERS spectrum) = 10.4 × (1.1×10^{13} molecules)/(1.8×10^{6} molecules) = 6.4×10^{7}].

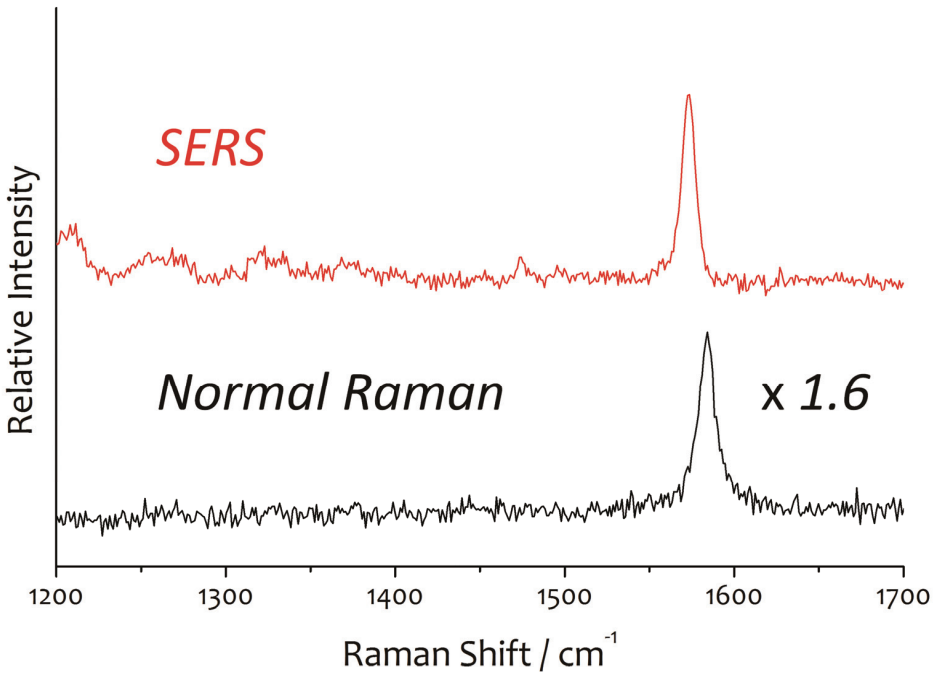

Figure 29. Comparison of the normal Raman spectrum of pure benzenethiol liquid with the SERS spectrum measured from the SERS substrate prepared by the four-step immobilization method. The acquisition time was 1 s. Spectra were acquired at 514.5 nm using a 10× objective (NA = 0.25).

Calculation of the average SERS enhancement measured from the substrate prepared by the four-step method.

In Figure 29, the ratio of the SERS intensity to the normal Raman intensity was about 1.6. Therefore, the enhancement factor is calculated to be approximately 9.8×10^{6} [= intensity ratio × (number of molecules irradiated in measuring the normal Raman spectrum)/(that for SERS spectrum) = 1.6 × (1.1×10^{13} molecules)/(1.8×10^{6} molecules)].

The molecules adsorbed on the isolated Ag colloidal particles could not contribute to the calculated enhancement, since the LSPR of them is near 390 nm, which is too far to be excited by a 514.5 nm light. Therefore, the actual enhancement on the dimers might be much higher than the calculated value. About 62 and 66% of the benzenethiol molecules were adsorbed on the dimers of the substrates prepared by the three- and four-step methods, respectively. If this factor is counted, the enhancement on the dimers becomes about 10.3×10^7 [= $6.4\times10^7/0.62$] for the substrate prepared by the three-step method. For the substrate prepared by the four-step method, it becomes about 1.5×10^7 [= $9.8\times10^6/0.66$]. The value of 1.5×10^7 corresponds to the enhancement outside the junctions, since no target molecules could present at the junctions of the dimers for the substrate prepared by the four-step method.

The enhancement measured from the substrate prepared by the three-step method was approximately 6.9 times stronger than that measured from the substrate prepared by the four-step method. As discussed in above, a certain portion of benzenethiol molecules would present inside the junctions of the dimers for the substrate prepared by the three-step method, while none inside the junctions for the substrate prepared by the four-step method. Therefore, the enhancement difference of 6.9 times is surely due to the contribution by the target molecules located inside the junctions. The percentage of the enhancement contributed by them is

calculated to be about 86% [=1−1/6.9×100%]. To calculate the enhancement inside the junctions, which act as the hotspots, it is necessary to know the amount of benzenethiol adsorbed on the surface area inside the junction regions. This amount could be estimated roughly if it is possible to know the surface area inside the junction regions where benzenethiol could not be adsorbed by diffusion. Unfortunately, any proper experiment methods to measure the surface area or theory to estimate it was not found. Therefore, it was assumed that benzenethiol molecules could not penetrate into the area whose gap is smaller than 1.4 nm, which corresponds to twice of the molecular size in the long axis (see Figure 30). Also, it was assumed that two colloidal particles were directly contacted, since the surface coverage of benzenethiol was very low as 3.6%. Actually, in the SEM images we can see that the two colloidal particles composing each dimer are in contact with each other. In some cases, they appear to be overlapping (see Figure 23). The surface of the spherical cap corresponding to the junction area is given as $2\pi rh$. Where r is the radius of the colloidal spheres and h is the height of the spherical cap. h is 0.7 nm for the gap of 1.4 nm. By this model, the percent of the junction area is about 2.5% of the total surface area of the colloidal particle [= $2\pi rh/4\pi r^2$ where r = 14 nm and h = 0.7 nm]. Since the number of target molecules adsorbed on the surface inside the junction regions is proportional to its surface area, the enhancement inside the junction regions is estimated at about 3.5×10^9 [= 10.3×10^7 × 86% /

2.5%]. [It should be mentioned that a minor correction by the surface area of the colloidal particles contacted on the P4VP film was ignored in the calculation.] In this calculation, the enhancement inside the junction regions is critically affected by the surface area inside the junction regions where benzenethiol could not be adsorbed by diffusion. If benzenethiol molecules could not penetrate into the area whose gap is smaller than 0.7 nm that corresponds to the molecular size in the long axis, the enhancement inside the junction regions becomes double. Therefore, there is no doubt that the enhancement value of 3.5×10^{9} is only a very rough estimation. An accurate method to figure out the surface area inside the junction regions where benzenethiol could not be adsorbed by diffusion is needed.

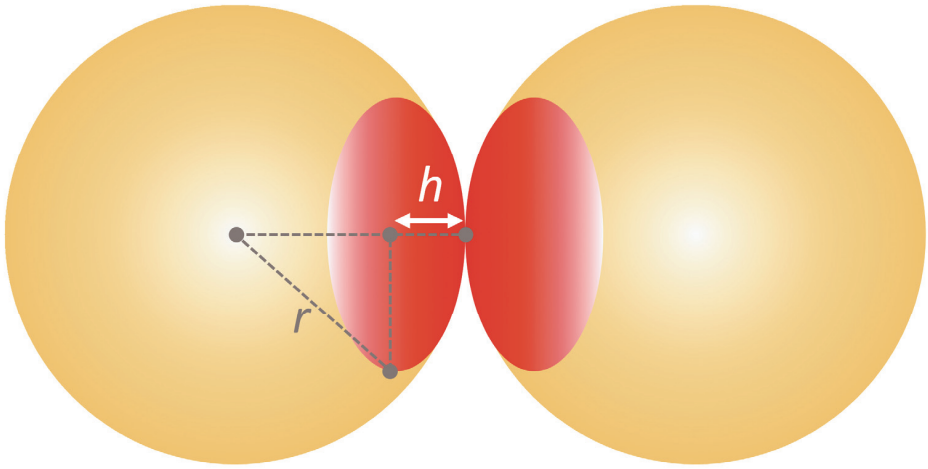

Figure 30. A schematic showing our approach to estimate the number of target molecules adsorbed on the surface of the junction of a dimer. The junction area is assumed to comprise a cap on the surface of each colloidal particle in the interparticle region of the dimer (red color).

5.2. Conclusions

Two kinds of SERS substrates were prepared by using the three- and four-step immobilization methods. By using purified Ag sols in the immobilizations, the dimers of Ag colloidal particles predominantly can be fabricated with forming very few trimers. The net surface charge of the colloidal particles was increased by purification, and the force of repulsion between the colloidal particles was increased significantly. Consequently, the dimers formed from the purified colloidal particles might have surface charge densities high enough prevent the attachment of new purified colloidal particles to them, and very few trimers were formed. Both substrates gave good SERS spectra. However, the spectral intensity measured from the substrate prepared by the three-step method was about 6.5 times higher than that measured from the substrate prepared by the four-step method. This was due to the fact that some of the target molecules could be present inside the junction regions for the substrate prepared by the three-step method, while none inside the junction regions for the one prepared by the four-step method. From the SERS intensity difference, the enhancement factors inside and outside the junction regions of the dimers of Ag colloidal particles could be distinctly calculated. It was found to be very roughly 3.5×10^{9} inside the junctions, while 1.5×10^{7} outside the junctions.

Chapter 6. Universal SERS-substrates

A method to fabricate sensitive and stable substrates that can be used in routine surface-enhanced Raman scattering spectral measurements was developed. The substrates were fabricated by immobilization of Ag colloidal particles on a glass plate coated with P4VP, adsorption of molecules on the immobilized colloidal particles, and second immobilization. In the second step, weakly adsorbed molecules such as aniline instead of target molecules were adsorbed. Pristine silver sols were purified by centrifuging to increase the surface charge of the colloidal particles and optimized Ag colloidal particle diameter to achieve high Raman signal enhancement from their dimers. When purified silver sols were used in the immobilizations, dimers were predominantly formed with very few trimers. When target molecular solutions were dropped in arrays on the substrate prepared by adsorbing aniline and dried, a good SERS spectrum was observed from each spot without any peaks of aniline and P4VP. The average enhancement was found to be 1.0×10^7 and the enhancement of the dimers was ~1.6×10^7. The latter corresponds to the enhancement outside the hotspot regions, since target molecules could not be adsorbed at the junctions after the formation of dimers. About one hundred samples could be tested on the substrate fabricated on a cover glass when target molecular solutions were dropped by using a micropipette. Since dropping and drying are very simple and easy processes, and many samples could be tested on a substrate, these substrates can be used in

routine SERS spectral measurements and assays like bioassays.

6.1. Results and Discussion

Figure 31 shows the SEM images and UV−Vis extinction spectra of the substrates prepared by the three−step immobilization method and adsorption of aniline in the second step, and the histogram of the number of Ag colloidal clusters counted from the SEM images. The Ag colloidal particles were first immobilized for 10 min on a cover glass coated with P4VP. [The density of Ag colloidal particles immobilized by the first immobilization affected to the density of the dimers formed during the second immobilization step. For a high density of the dimers without forming trimers, the average gap distance between the particles immobilized during the first immobilization should be larger than two times of the diameter of the particles and less than three times. When the first immobilization time was 10 min, the dimers were formed with a high density without forming the trimers significantly.] After immobilizing, the substrate was placed for adsorption of aniline in a 3.0 mL ethanol solution of aniline (200 nM) for 2 h. [The amount of aniline adsorbed on the Ag colloidal particles immobilized was not significantly affected to the formation of the dimers compared to the first immobilization time.] After adsorption aniline, the Ag colloidal particles were immobilized again on the substrate for various times. For both the immobilization steps, silver sols purified by centrifuging were used. After the purification, the ions and

molecules present in the pristine colloidal solutions were largely removed, and the surface charge of the colloidal particles was increased significantly. As a result, Ag colloidal particles were immobilized individually without any aggregation during the first immobilization (see Figure 31a). It is believed that no aggregation was due to the increased repulsion force between Ag colloidal particles whose surface charge was increased by purification. For the Ag colloidal particles immobilized in isolation, a single LSPR peak is observed at 390 nm in the extinction spectrum (see Figure 31e). On the other hand, dimers of Ag colloidal particles were formed predominantly and very few trimers during the second immobilization. The number of the dimers was increased with an increase in the second immobilization time but not linearly. The total number of the monomers and dimers after the second immobilization is larger than that of the monomers after the first one. This is due to that some colloidal particles were adsorbed individually even during the second immobilization. From the SEM images, we can see that the two colloidal particles composing each dimer are in contact with each other. In some cases, they appear to be overlapping. The dimers of Ag colloidal particles showed two LSPR peaks at 380 and 519 nm. The former peak is attributed to the transverse mode, while the latter is attributed to the longitudinal mode.[51,52] With an increase in the second immobilization time up to 30 min, the intensity of both the peaks increased without any shift in their extinction peak wavelengths (λ_{max}).

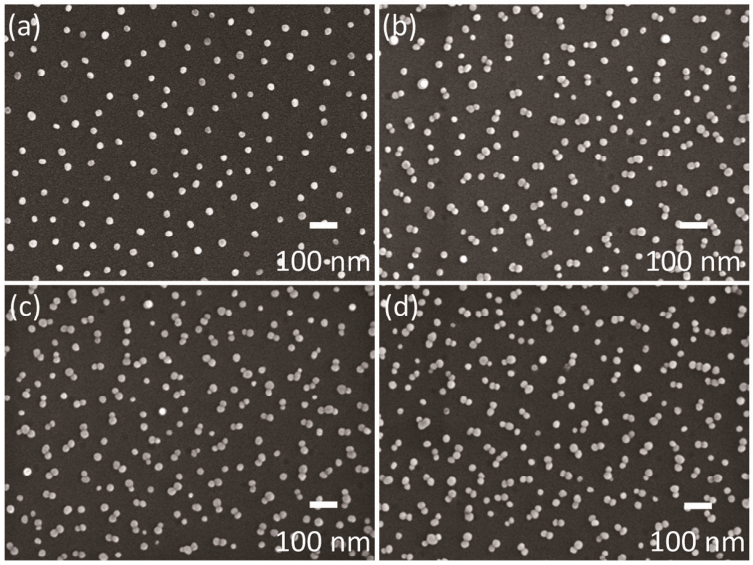
(a)
100 nm
(b)
100 nm
(c)
100 nm
(d)
100 nm

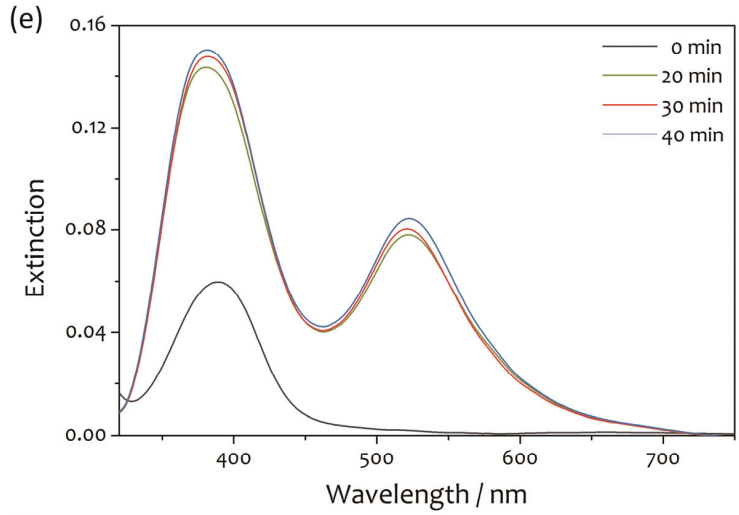
(e)
0.16
0.12
0.08
0.04
0.00
Extinction
400
500
600
700
Wavelength / nm
0 min
20 min
30 min
40 min

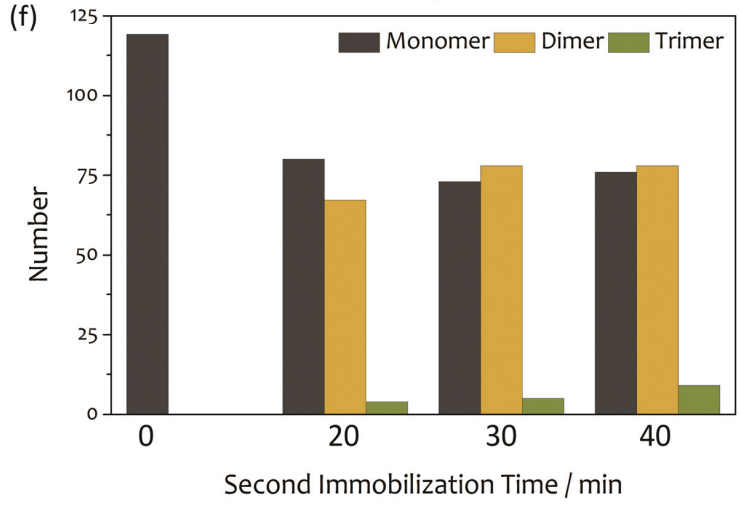
(f)
125
100
75
50
25
0
Number
0
20
30
40
Second Immobilization Time / min
Monomer
Dimer
Trimer

Figure 31. (a-d) SEM images and (e) UV−Vis extinction spectra of substrates prepared by a three−step immobilization method and adsorption of aniline in the second step, and (f) histogram of the number of Ag colloidal clusters counted from the SEM images. The first immobilization time was all the same as 10 min, while the second immobilization times were (a) 0, (b) 20, (c) 30, and (d) 40 min. Purified silver sols whose colloidal particles had 28 nm in average diameter were used in the immobilizations. The legend shows the second immobilization times.

Consider the effect of purification of silver sols to the cluster formation. Silver sols are very stable without formation of precipitation because the colloidal particles have the same kind of surface charge, and hence repel each other. It should be noted that for the fabrication of silver sols used in this study, sodium citrate and silver nitrate were added as a stabilizer and reagent, respectively. In addition, sodium ascorbate and sodium borohydride were added as reducing agents. Therefore, the Ag colloidal particles of silver sols were surrounded by the ions present in the colloidal solutions such as citrate, nitrate, borate, sodium, etc., and their surface charge was reduced significantly. The pristine sols were purified by removing the supernatant obtained after centrifuging them, and then adding the same volume of distilled water to the residue left behind. Consequently, the concentration of the ions present in the colloidal solutions was significantly reduced

by purification. Therefore, the net surface charge of the colloidal particles increased and the repulsion force between the colloidal particles increased significantly. There is no doubt that the probability of their aggregation during the immobilization would decrease with an increase in the force of repulsion between the Ag colloidal particles. This is the reason why the Ag colloidal particles in the substrate prepared using purified silver sols were immobilized individually without any formation of clusters (Figure 31a). When molecules were adsorbed on Ag colloidal particles, the surface charge was reduced, and the force of repulsion between the colloidal particles reduced. This can result in the aggregation of colloidal particles. Actually, dimers were formed predominantly, while trimers very few, during the second immobilization after the adsorption of aniline (see Figures 31b–d). However, when pristine silver sols were used in the immobilization, colloidal particle clusters such as dimers, trimers, and tetramers were formed randomly during the second immobilization (see ref. 47 and Figure 24). Therefore, it is concluded that the formation of trimers and tetramers is prohibited when purified silver sols are used in the immobilization. This may be related to the surface charge of the dimers formed. Since the Ag colloidal particles in the purified silver sols had a relatively higher surface charge than that in the pristine sols, it can be expected that the dimers formed from the purified colloidal particles had a higher surface charge than that formed from the pristine ones. Therefore, it is believed that the dimers formed

from the purified colloidal particles had surface charge densities high enough prevent the attachment of new purified colloidal particles to them. Hence, very few larger clusters such as trimers and tetramers were formed when purified silver sols were used in the immobilization steps.

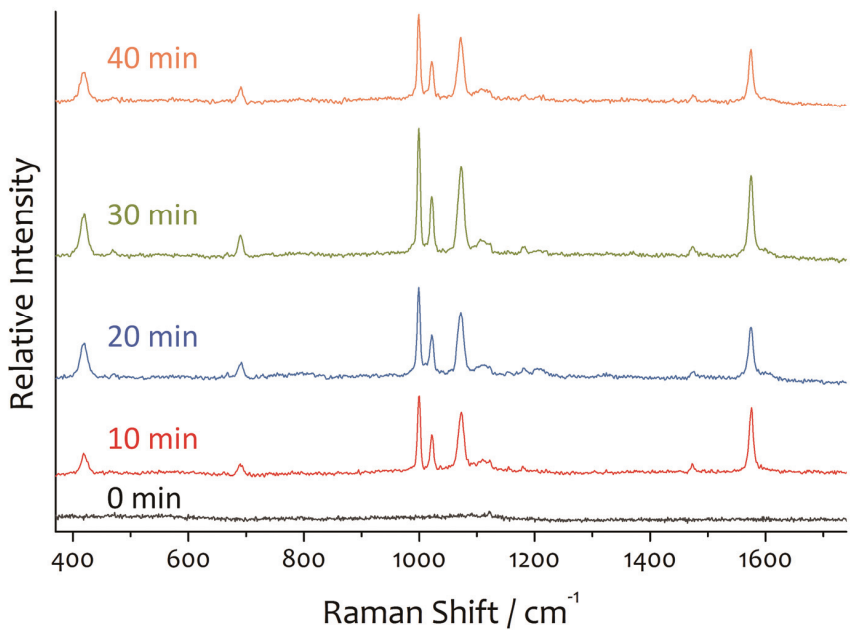

Figure 32. SERS spectra of benzenethiol measured from substrates prepared by a three-step immobilization method and adsorption aniline in the second step, after dipping each substrate in a 3.0 mL ethanol solution of 100 nM benzenethiol for 24 h and drying. The first immobilization time was all the same as 10 min, and the second immobilization time was varied. The legend shows the second immobilization times. A 514.5 nm Ar-ion laser line was used as the excitation source. The acquisition time was 1 s.

Figure 32 shows the SERS spectra of benzenethiol measured from the substrates prepared by the three-step immobilization method and adsorption of aniline in the second step, after dipping each substrate in a 3.0 mL ethanol solution of 100 nM benzenethiol for 24 h and drying. The first immobilization time was all the same as 10 min, and the second immobilization time was varied from 0 to 40 min with a 10 min step. All the spectra are well characterized and have all the same spectral shape. The distinct peaks in the SERS spectra correspond to the modes of the benzene ring of benzenethiol.[48] For example, the peak at 1573 cm^{-1} corresponds to ν_{8a}, while that at 1000 cm^{-1} corresponds to ν_{12}. The peak at 417 cm^{-1} corresponds to ν_{7a} and contributions from the C-S stretching vibration (ν_{CS}). It should be noted that no peaks corresponding to aniline and P4VP were observed. The highest intensity was observed from the substrate whose second immobilization was 30 min. The SERS intensity increased with an increase in the number of dimers but decreased with red-shifting the λ_{max} from 519 nm by increasing the number of larger clusters like trimers and tetramers at longer second immobilization times. The standard deviation of relative intensities measured at 10 different points of each sample was less than 5% when a laser beam with a diameter of ~1 μm was used (see Figure 33 and Table 3).

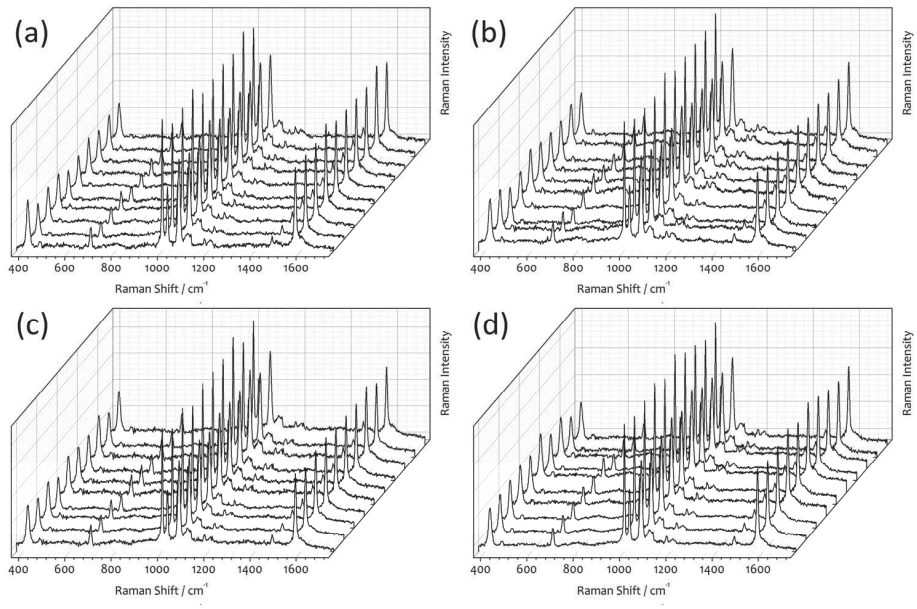

Figure 33. SERS spectra of benzenethiol obtained at 10 randomly selected positions within the substrates whose second immobilization time was (a) 10, (b) 20, (c) 30, and (d) 40 min. The acquisition time was 1 s.

	1	2	3	4	5	6	7	8	9	10	RSD(%)
10 min	421	434	417	426	441	442	443	476	449	470	4.38
20 min	550	543	494	525	526	505	537	499	527	558	4.11
30 min	655	649	721	710	689	680	682	684	660	723	3.84
40 min	431	437	422	463	475	467	485	468	469	465	4.52

Table 3. Experimental evaluation of relative standard deviation (RSD) of SERS intensity on the four different substrates whose second immobilization time was (a) 10, (b) 20, (c) 30, and (d) 40 min.

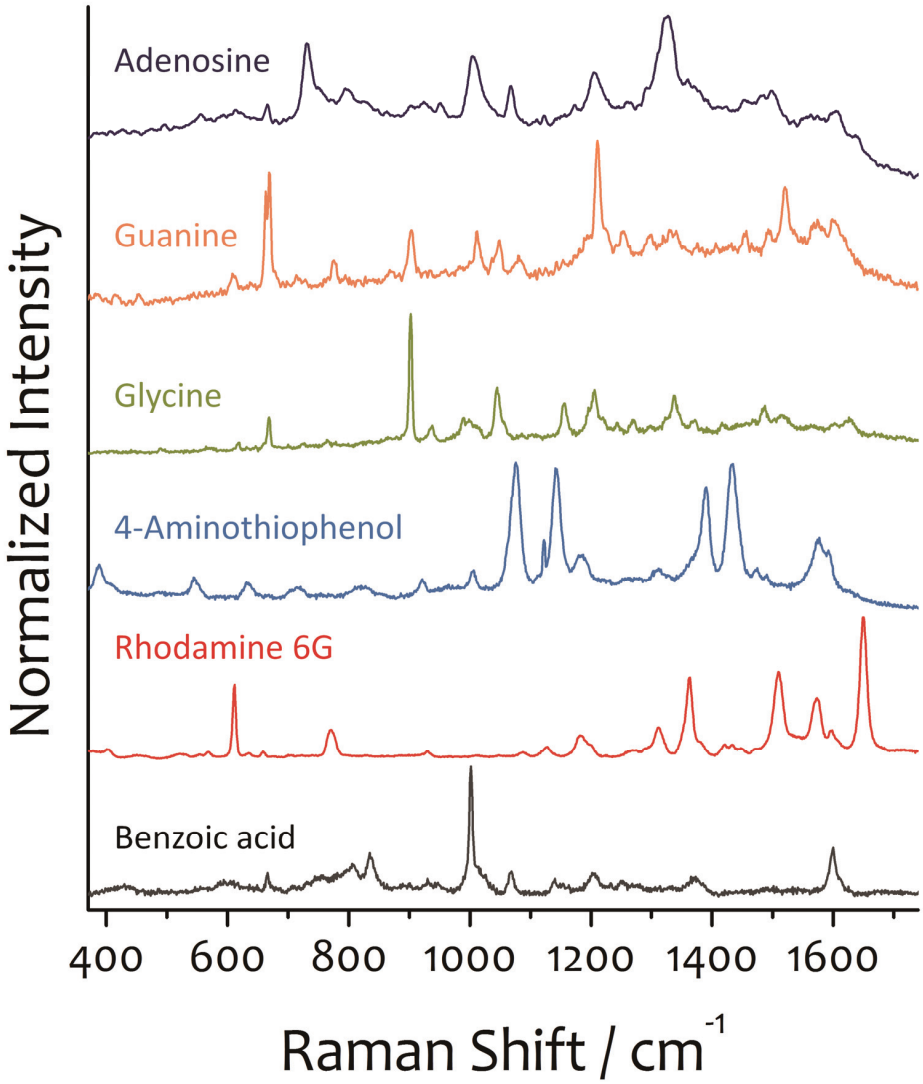

Figure 34. SERS spectra of several molecules measured from the spots after dropping target molecular solutions in arrays on the substrate, which was prepared by a three-step immobilization method and adsorbing aniline in the second step, and drying. The first and second immobilization times were 10 and 30 min, respectively. A 20 μL of target molecular solutions (100 nM) was dropped by using a micropipette. A 514.5 nm Ar-ion laser line was used as the excitation source. The acquisition time was 1 and 10 s for the bottom three molecules and the others, respectively.

Figure 34 shows the SERS spectra recorded from the spots after dropping several target molecular solutions in arrays on the substrate prepared by the three-step immobilization and adsorption of aniline in the second step, and drying. The first and second immobilization times were 10 and 30 min, respectively. In the second step, the substrate was placed in a 3.0 mL ethanol solution of aniline (200 nM) for 2 h. 20 μL target molecular solutions (100 nM) were dropped by using a micropipette. Each spot produced a very good SERS spectrum. No peaks corresponding to aniline and P4VP were appeared. The spectrum of aniline was very weak (see Figure 35). The SERS spectra of the target molecules are well agreed with reported SERS spectra.[48,53,54,55,56,57] For comparison purposes, the SERS spectra after dipping the substrates prepared by adsorbing aniline in each target molecular solution were also measured (see Figure 35). The SERS spectra measured after dropping were slightly better in the signal to noise ratio than those measured after dipping. This might be due to a different surface concentration of target molecules between two samples prepared by dipping and dropping.

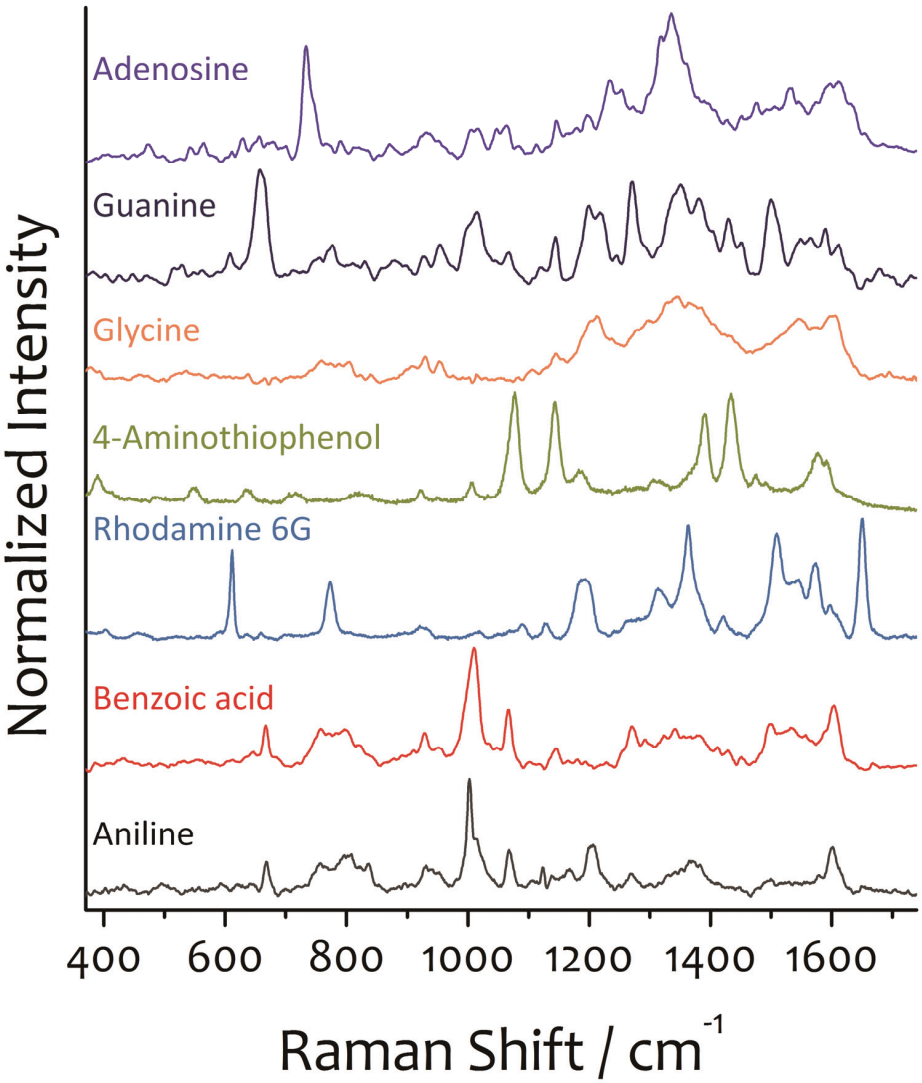

Figure 35. SERS spectra of several molecules, which were recorded from the substrates prepared by adsorbing aniline after dipping each substrate in a 3 mL of target molecule ethanol solution of each kind of target molecules. The first and second immobilization time were 10 and 30 min, respectively. Purified silver sols whose colloidal particles had 28 nm in average diameter were used in the immobilization steps. The concentration of target molecular solutions was all the same as 100 nM. A 514.5 nm Ar−ion laser line was used as the excitation source. The spectrum of aniline was

observed from the substrate prepared by adsorption of aniline, without any dipping or dropping. The acquisition time was 10 s for adenosine, guanine, and glycine and 1 s for the others.

The average enhancement of our universal SERS substrates is ~1.0×10^7. This value is about one order higher than that of the substrates prepared by the three-step immobilization method and using unpurified silver sols whose colloidal diameters were not optimized.[47] After dropping the target molecular solutions on our substrates and drying, very good SERS spectra were observed. Therefore, it can be concluded that the substrate prepared by adsorption aniline has a high enough sensitivity for qualitative SERS spectral measurements. A block of 2 mm × 2 mm was large enough to load a sample solution by dropping using a micropipette without overlapping with the nearest neighbor blocks and the SERS spectrum was obtained reliably from each block. Since the substrate fabricated on a cover glass (2.2 cm × 2.2 cm) could be divided into 11 × 11 sampling blocks (2 mm × 2 mm in unit size), about one hundred samples could be tested on the substrate. Therefore, our substrates can be used in assays such as bioassays. Since dropping and drying are very simple and easy processes and many samples could be tested on a substrate, the substrates can be used in routine SERS spectral measurements. In this aspect, the substrates can be called as universal SERS substrates.

6.2. Conclusions

A simple method to fabricate sensitive and stable SERS substrates that can be used conveniently in routine SERS spectral measurements and assays such as bioassays was developed. In the fabrication of SERS substrates by the three-step immobilization method, aniline was adsorbed, which is a weakly adsorbed molecule on Ag, instead of target molecules in the second step. To increase the surface charge of Ag colloidal particles, pristine silver sols were purified by centrifuging. When silver sols purified by centrifuging were used in the immobilization, the dimers of Ag colloidal particles were formed predominantly with very few trimers. It is concluded that the formation of trimers and tetramers is prohibited when purified silver sols are used in the immobilization. This is possible when the dimers formed from the purified colloidal particles have surface charge densities high enough prevent the attachment of new purified colloidal particles to them. A good SERS spectrum was observed from each spot when target molecular solutions were dropped in arrays on the substrate prepared by adsorbing aniline and dried. The enhancement of the dimers was found to be 1.6×10^{7}, which corresponded to the enhancement outside the junctions. Since dropping and drying are very simple and easy processes and many samples could be tested on a substrate, the substrates fabricated by adsorption of aniline can be used conveniently in routine SERS spectral measurements and assays such as bioassays.

References

1. Bütler, H. J. *et al.* Using Raman spectroscopy to characterise biological materials. *Nat. Protoc.* **11,** 1–47 (2016).
2. Schlücker, S. Surface-enhanced raman spectroscopy: Concepts and chemical applications. *Angew. Chemie - Int. Ed.* **53,** 4756–4795 (2014).
3. Sharma, B., Frontiera, R. R., Henry, A.-I., Ringe, E. & Van Duyne, R. P. SERS: Materials, applications, and the future. *Mater. Today* **15,** 16–25 (2012).
4. Schlücker, S. *et al.* Immuno-Raman microspectroscopy: In situ detection of antigens in tissue specimens by surface-enhanced Raman scattering. *J. Raman Spectrosc.* **37,** 719–721 (2006).
5. Schütz, M., Steinigeweg, D., Salehi, M., Kömpe, K. & Schlücker, S. Hydrophilically stabilized gold nanostars as SERS labels for tissue imaging of the tumor suppressor p63 by immuno-SERS microscopy. *Chem. Commun.* **47,** 4216 (2011).
6. Qian, X. *et al.* In vivo tumor targeting and spectroscopic detection with surface-enhanced Raman nanoparticle tags. *Nat. Biotechnol.* **26,** 83–90 (2007).
7. Lyandres, O. *et al.* Real-time glucose sensing by surface-enhanced Raman spectroscopy in bovine plasma facilitated by a mixed decanethiol/mercaptohexanol partition layer. *Anal. Chem.* **77,** 6134–6139 (2005).
8. Chou, I.-H. *et al.* Nanofluidic Biosensing for β-Amyloid

Detection Using Surface Enhanced Raman Spectroscopy. *Nano Lett.* **8,** 1729–1735 (2008).

9. Wang, G. F. *et al.* Detection of the Potential Pancreatic Cancer Marker MUC4 in Serum Using Surface–Enhanced Raman Scattering. *Anal. Chem.* **83,** 2554–2561 (2011).
10. Granger, J. H., Granger, M. C., Firpo, M. A., Mulvihill, S. J. & Porter, M. D. Toward development of a surface–enhanced Raman scattering (SERS)–based cancer diagnostic immunoassay panel. *Analyst* **138,** 410–416 (2013).
11. Ling, X. *et al.* Can graphene be used as a substrate for Raman enhancement? *Nano Lett.* **10,** 553–561 (2010).
12. Li, L. *et al.* Metal oxide nanoparticle mediated enhanced Raman scattering and its use in direct monitoring of interfacial chemical reactions. *Nano Lett.* **12,** 4242–4246 (2012).
13. Lounis, S. D., Runnerstrom, E. L., Llordés, A. & Milliron, D. J. Defect chemistry and Plasmon physics of colloidal metal oxide Nanocrystals. *J. Phys. Chem. Lett.* **5,** 1564–1574 (2014).
14. Henry, A. I. *et al.* Correlated structure and optical property studies of plasmonic nanoparticles. *J. Phys. Chem. C* **115,** 9291–9305 (2011).
15. Haes A. J. & Duyne*, R. P. Van. A Nanoscale Optical Biosensor: Sensitivity and Selectivity of an Approach Based on the Localized Surface Plasmon Resonance Spectroscopy of Triangular Silver Nanoparticles. *J. Am. Chem. Soc.* **124,** 10596–10604 (2002).

16. Hiep, H. M., Yoshikawa, H., Saito, M. & Tamiya, E. An interference localized surface plasmon resonance biosensor based on the photonic structure of au nanoparticles and SiO2/Si multilayers. *ACS Nano* **3,** 446–452 (2009).

17. Lee, S., Mayer, K. M. & Hafner, J. H. Improved localized surface plasmon resonance immunoassay with gold bipyramid substrates. *Anal. Chem.* **81,** 4450–4455 (2009).

18. Mayer, K. M., Hao, F., Lee, S., Nordlander, P. & Hafner, J. H. A single molecule immunoassay by localized surface plasmon resonance. *Nanotechnology* **21,** 255503 (2010).

19. Yoo, S. Y. *et al.* Detection of the most common corneal dystrophies caused by BIGH3 gene point mutations using a multispot gold-capped nanoparticle array chip. *Anal. Chem.* **82,** 1349–1357 (2010).

20. Cheng, C. S., Chen, Y. Q. & Lu, C. J. Organic vapour sensing using localized surface plasmon resonance spectrum of metallic nanoparticles self assemble monolayer. *Talanta* **73,** 358–365 (2007).

21. Chen, K. J. & Lu, C. J. A vapor sensor array using multiple localized surface plasmon resonance bands in a single UV-vis spectrum. *Talanta* **81,** 1670–1675 (2010).

22. Nuopponen, M. & Tenhu, H. Gold Nanoparticles Protected with pH and Temperature-Sensitive Diblock Copolymers Gold Nanoparticles Protected with pH and Temperature-Sensitive Diblock Copolymers. *Society* **23,** 5352–5357 (2007).

23. Mack, N. H. *et al.* Optical transduction of chemical forces. *Nano Lett.* **7,** 733–737 (2007).

24. Choi, Y., Park, Y., Kang, T. & Lee, L. P. Selective and sensitive detection of metal ions by plasmonic resonance energy transfer–based nanospectroscopy. *Nat. Nanotechnol.* **4,** 742–746 (2009).

25. Jahn, M. *et al.* Plasmonic nanostructures for surface enhanced. *Analyst* **141,** 756–793 (2016).

26. Hartland, G. V. Optical studies of dynamics in noble metal nanostructures. *Chem. Rev.* **111,** 3858–3887 (2011).

27. Link, S., Wang, Z. L. & El–Sayed, M. a. Alloy Formation of Gold–Silver Nanoparticles and the Dependence of the Plasmon Absorption on Their Composition. *J. Phys. Chem. B* **103,** 3529–3533 (1999).

28. Lu, X., Rycenga, M., Skrabalak, S. E., Wiley, B. & Xia, Y. Chemical Synthesis of Novel Plasmonic Nanoparticles. *Annu. Rev. Phys. Chem.* **60,** 167–192 (2009).

29. Turkevich, J., Stevenson, P. C., & Hillier, J. A Study of the Nucleation and Growth Processes I N the Synthesis of Colloidal Gold. Discuss. *Faraday Soc.* **11,** 55–75 (1949).

30. Gallouzi, 69 I E, Brennan, C. M. & Steitz, J. A. Photoinduced Conversion of Silver Nanospheres to Nanoprisms. *Cancer Res. Eur. J. Biochem. J. Biol. Chem. Mol. Cell. Biol. J. Cell Biol. Trends Biochem. Sci. J. Cell Biol* **7,** 1348–2969 (1901).

31. Evanoff, D. D. & Chumanov, G. Synthesis and optical

properties of silver nanoparticles and arrays. *ChemPhysChem* **6,** 1221–1231 (2005).

32. Brust, M., Walker, M., Bethell, D., Schiffrin, D. J. & Whyman, R. Synthesis of Thiol-derivatised Gold Nanoparticles in. *Chem. Commun.* **0,** 801–802 (1994).

33. Qu, L. & Dai, L. Novel silver nanostructures from silver mirror reaction on reactive substrates. *J. Phys. Chem. B* **109,** 13985–13990 (2005).

34. Cason, J. P. & Roberts, C. B. Metallic Copper Nanoparticle Synthesis in AOT Reverse Micelles in Compressed Propane and Supercritical Ethane Solutions. *J. Phys. Chem. B* **104,** 1217–1221 (2000).

35. Amendola, V., Polizzi, S. & Meneghetti, M. Free silver nanoparticles synthesized by laser ablation in organic solvents and their easy functionalization. *Langmuir* **23,** 6766–6770 (2007).

36. Choi, S. H., Lee, S. H., Hwang, Y. M., Lee, K. P. & Kang, H. D. Interaction between the surface of the silver nanoparticles prepared by γ-irradiation and organic molecules containing thiol group. *Radiat. Phys. Chem.* **67,** 517–521 (2003).

37. Xu, X., Yin, Y., Ge, X., Wu, H. & Zhang, Z. g-Radiation synthesis of poly ž acrylic acid / – metal nanocomposites. *Materials Lett.* **37,** 354–358 (1998).

38. Andrews, M. P. & Ozin, G. a. Wrapping oligomers and polymers around metal atoms, metal clusters, and metal

colloids. *Chem. Mater.* **1,** 174–187 (1989).

39. Patel, K., Sundara Raj, B., Chen, Y. & Lou, X. Cytotoxicity of folic acid conjugated hollow silica nanoparticles toward Caco2 and 3T3 cells, with and without encapsulated DOX. *Colloids Surfaces B Biointerfaces* **140,** 213–222 (2016).
40. Shafer-Peltier, K. E., Haynes, C. L., Glucksberg, M. R. & Van Duyne, R. P. Toward a Glucose Biosensor Based on Surface-Enhanced Raman Scattering. *J. Am. Chem. Soc.* **125,** 588–593 (2002).
41. Riboh, J. C., Haes, A. J., McFarland, A. D., Yonzon, C. R. & Van Duyne, R. P. A nanoscale optical biosensor: Real-time immunoassay in physiological buffer enabled by improved nanoparticle adhesion. *J. Phys. Chem. B* **107,** 1772–1780 (2003).
42. Chen, J. *et al.* Gold nanocages: Engineering their structure for biomedical applications. *Adv. Mater.* **17,** 2255–2261 (2005).
43. Rosi, N. L. & Mirkin, C. A. Nanostructures in biodiagnostics. *Chem. Rev.* **105,** 1547–1562 (2005).
44. Steinigeweg, D. & Schlücker, S. Monodispersity and size control in the synthesis of 20–100 nm quasi-spherical silver nanoparticles by citrate and ascorbic acid reduction in glycerol–water mixtures. *Chem. Commun.* **48,** 8682 (2012).
45. Bastus, N. G., Comenge, J. & Puntes, V. Kinetically controlled seeded growth synthesis of citrate-stabilized gold nanoparticles of up to 200 nm: Size focusing versus ostwald

ripening. *Langmuir* **27,** 11098–11105 (2011).

46. Malynych, S., Luzinov, I. & Chumanov, G. Poly(vinyl pyridine) as a universal surface modifier for immobilization of nanoparticles. *J. Phys. Chem. B* **106,** 1280–1285 (2002).

47. Lee, S., Gu, G. H. & Suh, J. S. A simple method to fabricate silver colloid clusters for surface-enhanced Raman scattering. *Chem. Phys. Lett.* **511,** 121–125 (2011).

48. Osawa, M., Matsuda, N., Yoshii, K. & Uchida, I. Charge-Transfer Resonance Raman Process in Surface-Enhanced Raman-Scattering From P-Aminothiophenol Adsorbed on Silver - Herzberg-Teller Contribution. *J. Phys. Chem.* **98,** 12702–12707 (1994).

49. Nishijima, Y., Hashimoto, Y., Rosa, L., Khurgin, J. B. & Juodkazis, S. Scaling rules of SERS intensity. *Adv. Opt. Mater.* **4,** 382-388(2014).

50. Félidj, N. *et al.* Optimized surface-enhanced Raman scattering on gold nanoparticle arrays Optimized surface-enhanced Raman scattering on gold nanoparticle arrays. *Appl. Phys. Lett.* **82,** 3095 (2010).

51. Mahmoud, M. A. Overgrowth of Silver Nanodisks on a Substrate into Vertically Aligned Nanopillars for Chromatic Light Polarization. *ACS Appl. Mater. Interfaces* **8,** 23827–23836 (2016).

52. Kriege I. *et al.* Shedding Light on Vacancy-Doped Copper Chalcogenides: Shape-Controlled Synthesis, Optical

Properties, and Modeling of Copper Telluride Nanocrystals with Near-Infrared Plasmon Resonances. *ACS Nano* **7,** 4367–4377 (2013).

53. Kamińska, A. *et al.* Highly reproducible , stable and multiply regenerated surface-enhanced Raman scattering substrate for biomedical applications. *J. Mater. Chem.* **21,** 8662–8669 (2011).

54. Madzharova, F., Heiner, Z., Gu, M. & Kneipp, J. Surface-Enhanced Hyper-Raman Spectra of Adenine, Guanine, Cytosine, Thymine, and Uracil. *J. Phys. Chem. C* **120,** 15415–15423 (2016).

55. Leem, J., Kang, H. W., Ko, S. H. & Sung, H. J. Controllable Ag nanostructure patterning in a micro fl uidic channel for real-time SERS systems. *Nanoscale* **6,** 2895-2901 (2014).

56. Kwon, Y. J., Dong, H., Ahn, S. J., Kim, M. S. & Kim, K. Vibrational Spectroscopic Investigation of Benzoic Acid Adsorbed on Silver. *J. Phys. Chem.* **98,** 8481–8487 (1994).

57. Kim, N. H. & Kim, K. Surface-enhanced resonance Raman scattering of rhodamine 6G on Pt nanoaggregates. *J. Raman Spectrosc.* **36,** 623–628 (2005)

Abstract in Korean

국문 제목

윤혁진
화학부 물리화학전공
The Graduate School
Seoul National University

표면 증강 라만 산란 (surface-enhanced Raman scattering) 기술의 출현 이후로 많은 연구 그룹에서 제작하기 쉬우면서도 라만 신호를 크게 증가시킬 수 있고, 안정한 SERS 기판을 만들고자 연구를 하고 있다. 이 논문은 은 또는 금 콜로이드 입자의 표면 전하의 조절을 통하여 간단하면서도 효과적으로 금속 이중합체를 기판에 제작하는 연구와 SERS로의 응용 연구 내용을 담고 있다. 원심분리기를 이용하여 금속 콜로이드 입자 주변의 이온들을 제거하면 입자의 표면 전하를 제어가 가능하다. 3단계 흡착 방법으로 SERS 기판을 쉽게 제작이 가능한데, 여기서 3단계 흡착 방법은 다음과 같다. 콜로이드 입자의 흡착 단계, 표적 분자의 흡착 단계, 콜로이드 입자의 재흡착 단계. 제작된 SERS 기판은 표면의 형태는 주사현미경(SEM)으로 확인하였으며, 광학 성질은 UV-vis 분광기를 통하여 측정하였다. 실험 조건의 변경을 통해 최적화된 SERS 기판을 얻을 수

있었으며, 이 때 증강 인자 값은 ~6.1×10^{7}이었다.

은 나노입자의 직경이 SERS 증강에 주는 효과에 대한 연구를 하였다. 다양한 크기의 은 나노 입자는 씨앗 매개 합성법을 통하여 합성이 가능하였다. 대략 5~10 nm 크기의 은 씨앗 입자는 sodium citrate와 silver nitrate의 혼합 용액에 sodium borohydride 용액을 첨가하여 얻을 수 있다. 은 씨앗 입자 용액에 silver nitrate와 환원제로 사용되는 sodium ascorbate를 적당량 넣어 반응 시키면 씨앗 입자를 성장시킬 수 있다. 이 때에 씨앗 입자의 양을 조절하면 간단하게 다양한 크기의 은 나노 입자를 얻을 수 있다. 이 합성 방법을 이용하여, 평균 크기가 21, 25, 28, 31 nm의 은 나노 입자를 합성하였다. 은 나노입자의 크기와 형태는 투과 전자현미경을 통하여 확인하였다. 은 나노 입자의 크기가 증가할수록 표면 플라즈몬 흡수 밴드가 장파장쪽으로 이동하였다. SERS 신호 세기는 514.5 nm 파장의 레이저를 이용하여 측정하였으며, 은 나노 입자의 크기에 따라 SERS 증강 효과가 달라지는 것을 확인하였다. 가장 높은 SERS 신호 세기는 흡수 스펙트럼이 519 nm에 위치하는 기판에서 측정이 되었다. 이 SERS 기판은 평균 직경이 28 nm인 은 나노 입자를 이용하여 만든 기판이었으며, 이 값은 21, 25, 31 nm 로 동일하게 제작한 기판들보다 높은 증강 수치를 보였다.

3단계 흡착 방법과 4단계 흡착 방법을 이용하여 두 종류의 SERS 기판을 제작하여 이 기판들의 신호 세기의 차이를 통하여 전체 SERS 신호 중에서 이중합체 접합부에 위치한 분자들의 기여도는 약 85%라고 실험적으로 계산하였다. 이 때 4단계 흡착 방법은 콜로이드 흡착 단계, aniline 흡착 단계, 콜로이드 재흡착 단계, 표적 분자 흡착 단계로 구성되어 있으며, 3단계 흡착 방법과 다르게 금속 이중합체가 표적 분자 흡착보다 먼저 만들어진다는 것이 특징이다. 그리고 핫스팟으로 볼 수 있는 이중합체의 접합 부분에서의 증강인자는 약 $\sim 3\times10^{9}$ 이다.

마지막으로 aniline을 사용하여 만든 SERS 기판(4단계 흡착 방법)은 범용 SERS 기판으로 사용이 가능하다. 표적 분자 용액 (adenosine, guanine, glycine, rhodamine 6G, benzoic acid, 4-aminothiophenol)을 기판에 떨어뜨린 후 건조시켜 라만을 측정했을 때 높은 높은 신호 증강을 보이는 스펙트럼들을 얻을 수 있었다. 이 때 증강 인자 값은 $\sim 9.1\times10^{6}$이었다.

Keywords : 표면 증강 라만 산란, 귀금속 나노 입자, 국소 표면 플라즈몬 공명, 이중합체, 플라즈모닉스, 라만 분광학

Student Number : 2013-30906